11-3-2014

Exploration of Electrodeposition of Aluminum-Nickel Alloys and Multilayers in Organic Chloroaluminate Ionic Liquids

Ammar Bin Waqar
University of South Florida, abwaqar@mail.usf.edu

Exploration of Electrodeposition of Aluminum-Nickel Alloys and Multilayers in Organic Chloroaluminate Ionic Liquids

by

Ammar Bin Waqar

A thesis submitted in the partial fulfillment
of the requirements for the degree of
Master of Science in Mechanical Engineering
Department of Mechanical Engineering
College of Engineering
University of South Florida

Major Professor: Wenjun Cai, Ph.D.
Delcie Durham, Ph.D.
Alex A. Volinsky, Ph.D.

Date of Approval:
November 3, 2014

Keywords: Potentioamperometry, cyclic voltammetry, SEM, FIB

DEDICATION

To my dad.

ACKNOWLEDGMENTS

I would like to take this opportunity to express my earnest gratitude to my mentor and major advisor Dr. Wenjun Cai for providing me an opportunity to do research under her supervision. Her constant support, humble nature and motivation has driven me to go beyond my limits. I sincerely thank her for nurturing me.

I extend my gratitude to Dr. Delcie Durham and Dr. Alex A. Volinsky for being a part of my defense committee, whose inputs and guidance have been immensely helpful. I want to thank them for their valuable time.

I would like to thank the Nanotechnology Research and Education Center, Department of Mechanical Engineering and College of Engineering.

I would especially want to thank my research group fellows Hesham Mraied and Sina Izadi for taking out generous portions of time from their busy schedules to assist me with the characterization tools.

I would like to thank my loving parents and my family for their sacrifices, patience and encouragement.

I would like to thank Zoya for believing in me.

Lastly I would like to thank my dearest friends Chris, Emad, Ebru, Mehreen, Salman, Urvish and Utkarsh who have been my family here.

TABLE OF CONTENTS

LIST OF TABLES ii

LIST OF FIGURES iii

ABSTRACT v

CHAPTER 1: INTRODUCTION 1

CHAPTER 2: ELECTROCHEMICAL PROPERTIES OF $AlCl_3$-EMIM-$NiCl_2$ 4
- 2.1 Background 4
- 2.2 Materials and Experimental Procedure 6
  - 2.2.1 Working Environment 6
  - 2.2.2 Chemicals 7
  - 2.2.3 Electrodes 8
  - 2.2.4 Cell Setup 9
- 2.3 Electrolyte Preparation 10
  - 2.3.1 Pretreatment of EMIM 10
- 2.4 Results and Discussion 12
  - 2.4.1 Dissolution of $NiCl_2$ in $AlCl_3$-EMIM System 12
  - 2.4.2 Electrochemical Characteristics of the Electrolytes 16
  - 2.4.3 Effect of Working Electrode 19
- 2.5 Conclusions 23

CHAPTER 3: ELECTRODEPOSITION OF Al-Ni ALLOYS AND BILAYERS 24
- 3.1 Background 24
  - 3.1.1 Electrodeposition of Al-Ni Alloys in Chloroaluminate Melts 24
  - 3.1.2 Electrodeposition of Multilayered Al/Ni 25
- 3.2 Experimental Procedures 26
- 3.3 Results and Discussion 27
  - 3.3.1 Effect of Deposition Potential on Alloy Composition 27
  - 3.3.2 Scanning Electron Microscopy (SEM) – Surface Morphology 30
  - 3.3.3 X-Ray Diffraction (XRD) – Phase Identification 33
  - 3.3.4 Electrodeposition of Al/Ni Bilayers 34
- 3.4 Conclusions 37

CHAPTER 4: CONCLUSIONS AND FUTURE WORK 38

REFERENCES 39

LIST OF TABLES

Table 1. Selected standard reduction potentials. 22

Table 2. Electrodeposition parameters and composition of deposits. 28

LIST OF FIGURES

Figure 1. Photograph of MBRAUN LABstar glove box workstation. 7

Figure 2. A schematic of the electrochemical cell; CE, RE, and WE represents the counter, reference, and working electrodes respectively. 9

Figure 3. Photograph of 2:1 $AlCl_3$:EMIM electrolyte under agitation. 11

Figure 4. (a) Photograph of bright orange $AlCl_3$-EMIM-$NiCl_2$ suspension; (b) $AlCl_3$-EMIM-$NiCl_2$ with undissolved $NiCl_2$ at the bottom. 12

Figure 5. Photograph of $AlCl_3$-EMIM-$NiCl_2$ being heated and stirred in heating mantle at 80°C. 13

Figure 6. Photograph of basic $NiCl_2$-EMIM-$AlCl_3$ solution. 13

Figure 7. Photograph of acidic $AlCl_3$-EMIM-$NiCl_2$ solution. 14

Figure 8. (a) Purifying $AlCl_3$-EMIM-$NiCl_2$ with Al plate; (b) black powder on Al plate. 15

Figure 9. Photograph of black powder magnetically accumulated on stir rod. 15

Figure 10. A series of cyclic voltammograms on W electrodes measured with scan rate of 20 mV/s with a step size of 2 mV: (a) $AlCl_3$-EMIM; (b) $AlCl_3$-EMIM compared with $AlCl_3$-EMIM containing 0.024 mol l^{-1} $NiCl_2$; (c) $AlCl_3$-EMIM compared with $AlCl_3$-EMIM containing 0.026 mol l^{-1} $NiCl_2$; (d) $AlCl_3$-EMIM compared with $AlCl_3$-EMIM containing 0.1 mol l^{-1} $NiCl_2$. 17

Figure 11. A comparison of cyclic voltammograms on W electrodes in $AlCl_3$-EMIM, $AlCl_3$-EMIM containing 0.024 mol l^{-1} $NiCl_2$, $AlCl_3$-EMIM containing 0.026 mol l^{-1} $NiCl_2$ and $AlCl_3$-EMIM containing 0.1 mol l^{-1} $NiCl_2$ measured with scan rate of 20 mV/s with a step size of 2 mV. 18

Figure 12. A series of cyclic voltammograms on Cu electrodes measured with scan rate of 20 mV/s with a step size of 2 mV: (a) $AlCl_3$-EMIM; (b) $AlCl_3$-EMIM compared with $AlCl_3$-EMIM containing 0.024 mol l^{-1} $NiCl_2$; (c) $AlCl_3$-EMIM compared with $AlCl_3$-EMIM containing 0.026 mol l^{-1} $NiCl_2$; (d) $AlCl_3$-EMIM compared with $AlCl_3$-EMIM containing 0.1 mol l^{-1} $NiCl_2$. 20

Figure 13. A series of cyclic voltammograms measured with scan rate of 20 mV/s with a step size of 2 mV: (a) $AlCl_3$-EMIM on W vs. Cu; (b) $AlCl_3$-EMIM containing 0.024 mol l^{-1} $NiCl_2$ on W vs. Cu; (c) $AlCl_3$-EMIM containing 0.026 mol l^{-1} $NiCl_2$ on W vs. Cu; (d) $AlCl_3$-EMIM containing 0.1 mol l^{-1} $NiCl_2$ on W vs. Cu. 21

Figure 14. A comparison of cyclic voltammograms on Cu electrodes in $AlCl_3$-EMIM, $AlCl_3$-EMIM containing 0.024 mol l^{-1} $NiCl_2$, $AlCl_3$-EMIM containing 0.026 mol l^{-1} $NiCl_2$ and $AlCl_3$-EMIM containing 0.1 mol l^{-1} $NiCl_2$ measured with scan rate of 20 mV/s with a step size of 2 mV. 22

Figure 15. Schematic waveforms of (a) constant potential; (b) pulse potential. 27

Figure 16. Photograph of electrodeposited samples. 29

Figure 17. SEM images of (a) sample 1; (b) sample 2; (c) sample 3; (d) sample 5. 31

Figure 18. SEM image of sample 7. 31

Figure 19. SEM images of (a) pure Al deposit at -0.3 V in 1.5:1 M $AlCl_3$-EMIM containing 0.026 M $NiCl_2$; (b) pure Ni deposit at 0.4 V in 1.5:1 M $AlCl_3$-EMIM containing 0.1 M $NiCl_2$. 32

Figure 20. XRD patterns of sample 1 (a) full pattern (b) zoomed in detailed pattern. 33

Figure 21. SEM image of a FIB cross-section of Ni/Al bilayer sample. 35

Figure 22. Ion image of a FIB cross-section of Al/Ni bilayer sample. 36

ABSTRACT

Aluminum-nickel (Al-Ni) alloys and Al/Ni bilayers were successfully electrodeposited from $AlCl_3$-EMIM-$NiCl_2$ electrolyte at room temperature. Dissolution of $NiCl_2$ was shown to be favorable in Lewis basic (with molar ratio of $AlCl_3 < 0.5$) $AlCl_3$-EMIM solution. The use of electrochemically active Cu working electrode as opposed to inert W induced additional Cu oxidation and dissolution in the cyclic voltammetry scan. The reduction potentials of Al and Ni were found to be ~ -0.3 and 0.15 V vs. Al/Al^{3+} respectively. Increasing [$NiCl_2$] in the electrolyte leads to an increase of Ni concentration in the deposited structures. Dense and well-adherent Al-Ni alloys with Ni concentration up to 17.7 at.% were deposited by potential control. XRD analysis revealed that the deposited Al-Ni exhibit a supersaturated fcc crystalline structure. The visual appearance of the deposits ranged from bright silver, dull silver, grey, to black, where the darker shade typically indicated higher Ni content. SEM analysis revealed that the surface morphology of the deposits ranged from nodular to flake-like structures. Al-Ni alloy typically showed nodular morphology with cauliflower structure. Flake structures, which were independent of substrate roughness, were found to develop under pulsed potential deposition with 1:1 duty ratio.

The concentration of Ni in electrodeposited Al-Ni alloys increases nonlinearly with the increase in molarity of $NiCl_2$. Al and Ni contents increase with increasing the time of positive and negative cycle of the pulse respectively. Decreasing the frequency by half resulted in almost double the amount of Ni in the deposited alloy. A smoother substrate increased Ni concentration from 6 to 17.7 at.%. Al/Ni bilayer was successfully deposited in 1.5:1 $AlCl_3$-EMIM containing 0.026 M $NiCl_2$. Deposition of Al on Ni was achieved using constant potential and pulse potential control. The deposition of Ni on Al is complicated since the deposition potential of Ni lies in the vicinity of Al stripping potential thus inducing competition between Ni deposition and Al stripping.

CHAPTER 1: INTRODUCTION

Al, when alloyed with appropriate transition metals (TMs), exhibit excellent physical and mechanical properties [1]. Among various alloying elements, Ni is particularly interesting because Al-Ni exhibits excellent corrosion resistance, high temperature oxidation resistance, high strength, good ductility, and magnetic pertinence [2-7]. While traditional Al-based alloys are mostly crystalline in nature, recent developments in metallic glasses have sparkled great interest in developing Al-based metallic glass [2]. Transition metals such as Fe, Co, Ni or Cu are often used with rare earth metals to make Al-based metallic glasses. Among all TMs, Ni has the greatest effective amorphous alloy forming capability with Al, followed by Fe, Co, and Cu. Amorphization is closely related to reduced glass transition temperature (T_g/T_m) where T_g and T_m are the glass transition and melting temperature respectively. Glass forming ability (GFA) of these alloys is directly proportional to T_g/T_m. Strategies for synthesizing glass forming alloys developed over the years include Egami's volume strain criterion [8-10], Miracle's topological criterion [11, 12] and Inoue's three empirical rules [13, 14]. Inoue's rules state that,

1. the alloy system must consist of at least 3 components as the formation of amorphous phase becomes easier with increasing number of components
2. the atomic radius mismatch between the constituent elements must differ by 12% or more
3. there should be large negative heats of mixing between the components

For a binary system of Al with a late transition metal (LTM), Inoue's rule # 3 is best satisfied by Ni with a heat of mixing of -114 kJ mol^{-1} [15]. Thus Al-Ni alloy system is chosen for the purpose of this research.

Various processing techniques have been used to synthesize Al-Ni including physical vapor deposition (PVD) [16, 17], plasma assisted chemical vapor deposition (PACVD) [18, 19], hot pressing [20]

and electromagnetic stirring [21, 22]. Among these techniques, electrodeposition (ED) is the most economical and easy to scale-up technique which allows easy control of composition and phase of the deposit by adjusting deposition parameters including electrolyte composition, agitation, temperature and current/potential. Due to these characteristics, ED of Al and its alloys with various transition metals have been a topic of great interest among researchers for more than a century now. For these reasons, we focus on the ED process in this thesis.

However, ED of Al and its alloy is not very easy to perform. For the longest time, the Hall-Héroult process was used for the ED of Al in ores. The main drawbacks to this method is the process complication caused by the requirement of very high temperatures (950-1000°C) and pollutant emission [23-25]. Certain advancements in the Hall- Héroult process lowered this temperature to 900°C by adding 5 wt.% LiF in the electrolyte [26]. Also, Al cannot be deposited in aqueous solutions due to the evolution of hydrogen prior to the Al deposition process. ED in non-aqueous room temperature solutions or ionic liquids (ILs), on the other hand, provides a cost effective alternative due to recent developments. It has been the most researched topic in the field of ED of metals from ILs as compared to ED of other metals [27]. Aprotic non-aqueous electrolytes such as aluminum chloride ($AlCl3_3$) with 1-ethyl-3-methylimidazolium chloride (EMIM), N-[n-Butyl] pyridinium chloride (BPC), trimethylphenylammonium chloride (TMPAC) etc. have been successfully utilized to deposit Al [7, 23, 25, 28]. These room temperature ionic liquids and their ED capabilities have sparked tremendous excitement among researchers over the years. Due to their hygroscopic nature, many of these electrolytes must be used under inert environment. High temperature ionic liquids such as $AlCl_3$ with sodium chloride (NaCl) are also available. But their main disadvantage is the high vapor pressure of Al_2Cl_6 which is unfavorable for modern applications [29].

In addition to Al-Ni alloy system, another interesting application of these metals is the Al/Ni reactive multilayer system. These multilayers have a lot of advantages including easy ignition, self-sustaining exothermic synthesis after reaction, very high local temperatures upon propagation (around 1000°C) and zero emission making them environmental friendly [30, 31]. These characteristics make them

useful in applications such as soldering, welding, brazing, joining, sealing, ignition, local heat sourcing and propulsion [31, 32]. Researchers have fabricated these layers using cold rolling [33], sputtering [30, 31] and electron-beam deposition [34]. These methods have their own advantages but are either very expensive or not very efficient at producing continuous multilayers. Up till now, there has not been any reports of producing Al/Ni multilayers using ED in chloroaluminate molten salts.

There has been a lot of studies on the ED of Al but those of Al alloys, especially Al-Ni, are a few. For Al-Ni ED, $AlCl_3$-EMIM-$NiCl_2$ of desired molarity is required. Previous study suggests that $NiCl_2$ is difficult to dissolve in acidic $AlCl_3$-BPC while it was readily dissolved in basic melt [35]. However, there has only been a few studies on the behavior of the dissolution of $NiCl_2$ in $AlCl_3$-EMIM and its electrochemical properties.

Based on the observations mentioned above, this thesis seeks to study the electrochemistry of Al-Ni deposition, understand the structure-processing relationship, with an ultimate goal of producing electrodeposited Al-Ni and Al/Ni multilayers using $AlCl_3$-EMIM-$NiCl_2$ ionic liquid. The organization of this thesis is described with a brief introduction to the concerning chapters below,

- Chapter 2: This chapter deals with the study on the synthesis and electrochemical properties of $AlCl_3$-EMIM-$NiCl_2$ room temperature molten salt.
- Chapter 3: ED of Al-Ni alloy and bilayers in $AlCl_3$-EMIM-$NiCl_2$ is described in this chapter. The deposits are characterized based on microstructure, surface morphology, composition and phase identification.

CHAPTER 2: ELECTROCHEMICAL PROPERTIES OF $AlCl_3$-EMIM-$NiCl_2$

2.1 Background

Electrodeposition (ED) of metallic materials involves reduction of metal ions from a conductive electrolyte using an electric current or potential. The electrolyte is composed of cations and anions which act as charge carriers for the current. During metal ED, the cations are transferred to the cathode where they are reduced under the influence of an applied current or potential. In Ni deposition, Ni^{2+} is reduced according to the following reaction [29],

$$Ni^{2+}(solv) + 2e^- \rightarrow Ni. \quad (2.1)$$

Organic chloroaluminate molten salt synthesized by adding aluminum chloride ($AlCl_3$) to 1-ethyl-3-methylimidazolium chloride (EMIM) provides useful and attractive characteristics such as adjustable Lewis acidity, wide electrochemical window, aprotic nature, room temperature stability, good conductivity, and low vapor pressure [24, 29]. $AlCl_4^-$ and $Al_2Cl_7^-$ unsaturated species are present in the electrolyte while the concentration of the later increases with electrolyte acidity. The acid base characteristic of this melt is represented by the reaction [36],

$$2AlCl_4^- \leftrightarrow Al_2Cl_7^- + Cl^-. \quad (2.2)$$

In $AlCl_3$-EMIM electrolyte, Al ED can only be successful in acidic solution since the formation of the electroactive $Al_2Cl_7^-$ is formed only when the molar fraction of $AlCl_3$ becomes larger than 0.5. In basic $AlCl_3$-EMIM solutions, the only electroactive specie is $AlCl_4^-$, whose reduction potential is more negative than the breakdown potential of the organic cation from the electrolyte. The electrochemically active $Al_2Cl_7^-$ unsaturated ion reduces to Al at the cathode according to the following reaction [37],

$$4Al_2Cl_7^- + 3e^- \leftrightarrow Al + 7AlCl_4^-. \quad (2.3)$$

Tang and Azumi [38] experimented on depositing Al on Pt substrate in $AlCl_3$-EMIM melt using various polarization techniques to optimize the grain size and microstructure of the deposits. Current pulse method was found to produce dense and well adherent Al deposits with a smooth surface. An inverse dependence of grain size with the applied current density was confirmed using galvanostatic polarization. Monopolar current pulse method gave smooth surface deposits at higher current density. The bipolar current pulse polarization was endorsed since it ameliorated the adhesion capability of the deposits in addition to enhanced smoothness and density of the deposits. Jiang et al. [24] studied ED of Al using $AlCl_3$-EMIM on Al substrates since they have high current densities to target recycling of Al. Electrical conductivities of 1.5:1 and 2:1 molar ratio $AlCl_3$-EMIM melt increase with temperature. Constant potential controlled ED of Al at potentials from -0.1 to -0.4 V yielded dense and continuous deposits at 60°C. Constant current controlled deposition at 90°C produced dense and well adherent deposits from 10 to 100 $mA{\cdot}cm^{-2}$ and loosely adherent deposits when current densities exceeds 100 $mA.cm^{-2}$. Liao et al. [28] carried out ED of Al on Cu in $AlCl_3$-EMIM melts with benzene added as a cosolvent. The addition of benzene in the melt enhanced the quality of the deposit by greatly reducing the viscosity and increasing the conductivity of the electrolyte. Current controlled electrolysis with current densities ranging from 0.75 to 7.54 $mA.cm^{-2}$ was used to deposit Al. They observed a decrease in the crystallite size with the increase in the current density and a transition from dull grey to white color of the deposit when the molar ratio of the melt is changed from 2:1 to 1.5:1.

The microstructure of the electrodeposited Al was characterized by Jiang et al. [24] to change from fine and dense crystallites to a dendritic structure upon increasing the current density above 100 $mA{\cdot}cm^{-2}$. They also found that the aluminum crystallites size decreased as the current densities increased. Similar dense Al deposits with a smooth structure and equiaxed grains at higher current densities were also reported in other works [28]. ED of Al is widely considered to follow a two stage process starting with initial nucleation followed by deposit growth [38].

Ni deposition in chloroaluminate melts is an area of great interest among researchers. Deng et al. [39] studied the ED characteristics of Ni in 1-ethyl-3-methylimidazolium dicyanamide (EMIM-DCA) with $AlCl_3$ and $NiCl_2$ glassy carbon and Cu substrates. Cyclic voltammetry study revealed the nickel reduction peak at -1.6 V. Deposition potential greatly influenced the microstructure and morphology of the deposits. Dense and compact deposits were obtained at potentials of -1.4 V while cracks start to develop at potentials around -1.5 V. Ni deposited at -1.6 V showed a coarse cauliflower structure due to high deposition rate. The surface roughness measured by AFM was 16 nm for -1.4 V deposition potential and increased to 90 nm at -1.6 V. The deposition of Ni was considered to follow a three dimensional progressive nucleation with diffusion controlled growth on both the electrodes. X-Ray diffraction revealed the presence of a crystalline structure with Al (111) and Ni (200).

Although ED of Al and Ni are well researched, which also entails the study of the electrochemical properties and synthesis of the electrolyte, a comprehensive study on the synthesis, electrochemical properties of $AlCl_3$-EMIM-$NiCl_2$ and the effect of the working electrode (WE) on the reduction and oxidation peaks is required. This chapter aims to address these issues.

2.2 Materials and Experimental Procedure

2.2.1 Working Environment

The chemicals used in the ED are highly sensitive to moisture and O_2. Thus an inert environment is required to prevent chemical degradation and provide a stable environment for all the reactions. MBRAUN LABstar Glove Box Workstation (shown in Figure 1) was utilized for all environment-sensitive processes. This Ar-filled glove box is capable of maintaining H_2O < 1 ppm and O_2 < 1 ppm through a compact gas purification system while also sustaining the desired pressure level. All experiments inside the glove box were carried out in the 2 to 4 mBar pressure range while the chemicals were stored at 8 to 12 mBar in idle state.

Figure 1. Photograph of MBRAUN LABstar glove box workstation.

2.2.2 Chemicals

The synthesis of the electrolyte for the desired ED process requires moisture and O_2 sensitive chemicals including Lewis acids and bases. Acidic metal bases including anhydrous aluminum chloride ($AlCl_3$, 99.999%, Aldrich) and anhydrous Nickel chloride ($NiCl_2$, 99%, Alfa Aesar) were used as-received. 1-Ethyl-3-methylimidazolium chloride (EMIM, >98% , Iolitec) were purified similar to previous work to be used as bases [40]. All the chemicals were kept in inert and dry conditions all the time. EMIM is highly sensitive to air and moisture. In general, as-received EMIM is purified prior to ED to remove excess moisture. The most extensively used method for the pretreatment and purification of EMIM was previously described [40]. This method and variations of it developed over the years involves heating EMIM for 2 or more days at 60 to 75 °C under vacuum. Another method described in the literature comprises of heating the EMIM at 100 °C for 24 hours [38]. Both variations of the heat treatment of EMIM to remove excess moisture were exercised and tested in this research.

2.2.3 Electrodes

The nature of electrodes in ED process plays a major role in the quality and characteristics of the deposits. Li et al. [41] studied the effect of various WEs including glassy carbon (GC), W, Ni, Al and Cu during Al ED in inorganic chloroaluminate molten salt $NaAlCl_4$ electrolytes at 175°C. Cyclic voltammograms (CV) of these systems with potential sweeps ranging from around 2 to -0.2 V were used to exam the different behaviors of these WEs. It was found that GC and W WEs were electrochemically inert during the complete CV scan whereas Ni substrate formed $NiCl_2$ at 1 V according to the following reaction,

$$Ni + 2Cl^- \leftrightarrow NiCl_2 + 2e^-. \quad (2.4)$$

Also, the deposits on the GC WE were found to be discontinuous with poor adhesion. Cu WE was highly active and continuously dissolved in the melt at potentials higher than 0.2 V. For Al WE, Al reduction initiated at 0 V. Ni and W WEs were suggested for Al/NaCl-$AlCl_3$/Ni battery system as they showed better reversibility of deposition and stripping. To test the effects of both an inert and electrochemically active substrate on the characteristics of the electrolyte, W and Cu were selected as WEs for this research.

In the present work, Al plate (99.99%, Alfa Aesar) and Al wire (99.99%, Alfa Aesar) were used as the counter and reference electrodes respectively unless specified otherwise. Three different materials: Cu plate (99.99%, Online Metals, 25 x 15 x 1 mm), Al plate (99.99%, Alfa Aesar, 25 x 15 x 1 mm) and W wire (99.99%, Sigma Aldrich, 1 mm diameter) were employed as the working electrodes. The exposed area of Al and Cu WEs to the electrolyte was limited to 2.25 cm^2 by covering the rest of the area with epoxy or electrochemical stop liquor. Prior to deposition, Al electrodes were first polished with SiC paper of 180 grit, rinsed with water and dried with kimwipes. Afterwards they were treated by an acid solution of 70% H_3PO_4, 25% H_2SO_4 and 5% HNO_3 by volume for 10 minutes to remove the native oxides from the Al surface. Cu electrodes were pretreated in an acid solution of 10 % H_2SO_4 and 90% H_2O (by volume) for 30 seconds. Both electrodes were then cleaned with water, dried with kimwipes and transferred to the glove

box for immediate use. For W electrodes, mechanical polishing using 180 grit SiC paper was applied prior to ED.

2.2.4 Cell Setup

All ED and cyclic voltammetry experiments were performed in a typical three-electrode electrochemical cell using Gamry Reference 600 Potentiostat/Galvanostat/ZRA, as illustrated in Figure 2. The three electrodes: counter, reference and working electrodes were immersed in the beaker containing the melt. During ED, the distance between CE, RE, and WE was fixed by passing the connecting wire through holes in a rubber cork.

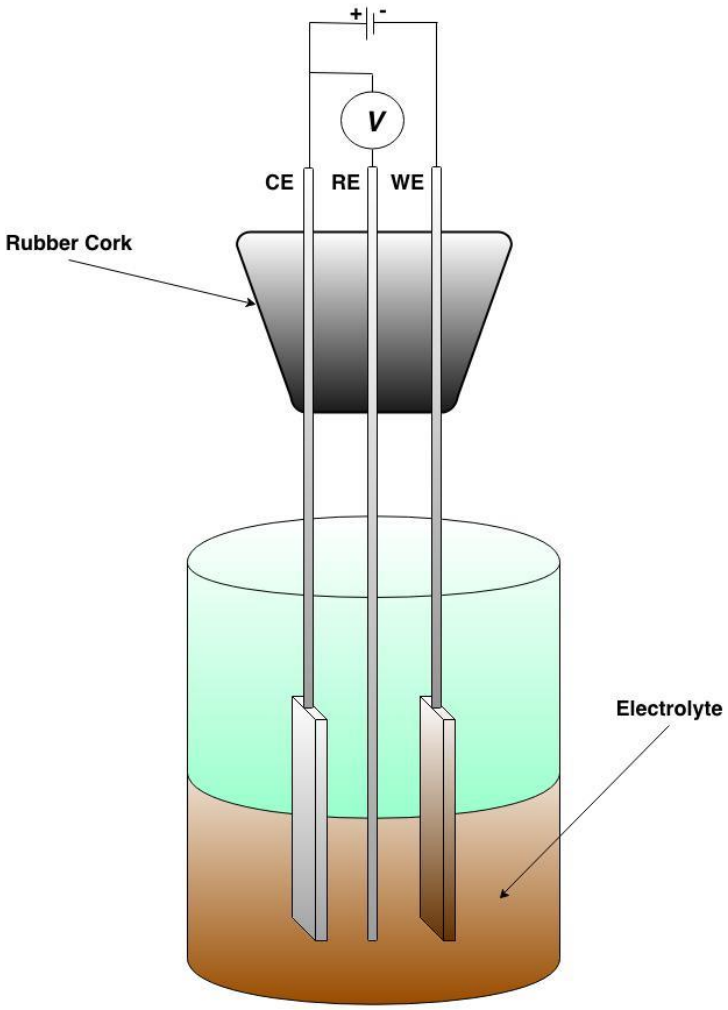

Figure 2. A schematic of the electrochemical cell; CE, RE, and WE represents the counter, reference, and working electrodes respectively.

2.3 Electrolyte Preparation

2.3.1 Pretreatment of EMIM

EMIM was first purified by heating it under vacuum (using Schlenk line) at 100°C for 24 hours [38]. This temperature is well above the melting temperature of EMIM (~ 77-79°C) thus the EMIM turns to liquid. After 24 hours of heating, upon removal of the flask from the heated oil bath, the melted EMIM crystallizes into solid. $AlCl_3$-EMIM was prepared by adding $AlCl_3$ to the crystallized EMIM in inert environment.

The acid and base for the reaction bear a solid state while their reaction produces a liquid electrolyte at room temperature. Initially 2:1 molar ratio $AlCl_3$-EMIM was synthesized and used for the ED process. EMIM (Aldrich, ≥95% pure) was heated at 100°C for 24 hours to remove moisture [38]. Upon addition of $AlCl_3$, the reaction produced white fumes and the O_2 level exceeded 20 ppm making it necessary to purge the glovebox while the reaction occurs. A vast majority of researchers heat EMIM at 60°C for 3 days. This method yielded relatively drier EMIM but the problem was found to lie with the EMIM out of the box. For this reason a higher purity EMIM (IL, >98% pure) was tested.

One of the features of a dry EMIM is a much lighter color, close to white while a dark yellow or deep pale color corresponds to the presence of moisture. Instead of being in the form of dry granules or powder, the EMIM (IL, >98% pure) supplied was moist and pale out of the box indicating the presence of moisture. To resolve this, a two-step preheat treatment was performed to remove excess moisture from the EMIM. The EMIM was first taken out of the bottle and placed in weighing pans inside the glove box. These EMIM were evenly spread out and left inside the glove box for several days to ensure maximized surface area exposure to increase the evaporation rate. After a few days, depending upon the level of moisture in the EMIM, the chemical becomes drier losing its moist texture, and sticks together to form a brittle network structure.

These dried EMIM were then ground in a mortar with a pestle to fine granules. The next preheat step included further heating these granules in Pyrex dishes at 40°C for several days (3 to 5) inside the glove box. The quantity of EMIM being heated in the dishes was carefully controlled making sure that the height of the spread out chemical does not exceed 2 to 3 mm to ensure uniform heating. The EMIM was taken out of the Pyrex dish and ground to finer granules every 24 hours to progressively increase the contact area of the grains. This increased the rate and efficiency of drying resulting in very fine dry EMIM grains already lighter in color. This preheated EMIM is now well suited for the heating process.

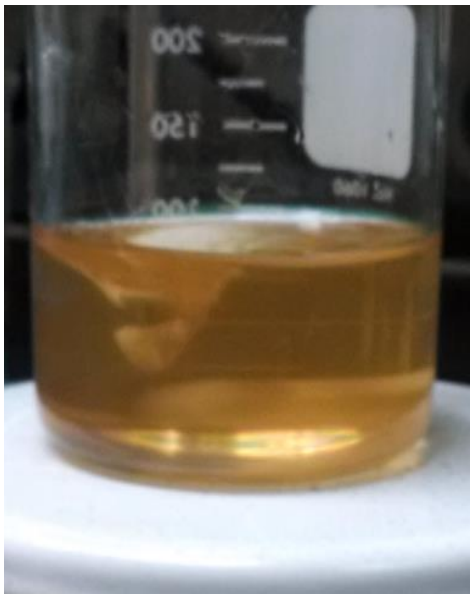

Figure 3. Photograph of 2:1 $AlCl_3$:EMIM electrolyte under agitation.

The heating chosen for the purpose of this research is 60°C for 3 days in an oil bath being the most widely used technique. The resultant EMIM has a much whiter color indicating very low moisture content. The heated EMIM was left for a few hours to cool down and then transferred back to the glove box where $AlCl_3$ was introduced to form 2:1 molar ratio $AlCl_3$-EMIM electrolyte. The O_2 level in the glove box only increased from <0.1 to 0.3 ppm which is almost negligible proving the effectiveness of the preheat treatment. The electrolyte prepared was dark yellow in color. Further purification of the electrolyte was carried out by stirring the electrolyte with a pure Al plate immersed in the liquid electrolyte for 3 days. The purified electrolyte appeared to be light yellow in color as shown in Figure 3.

2.4 Results and Discussion

2.4.1 Dissolution of $NiCl_2$ in $AlCl_3$-EMIM System

For Al-Ni deposition, the introduction of active Ni^{2+} ions in the electrolyte is required. Previous study suggests that $NiCl_2$ is difficult to dissolve in acidic $AlCl_3$-BPC while it was readily dissolved in basic melt [35]. To study the dissolution behavior of $NiCl_2$ in $AlCl_3$-EMIM, 0.01 M $NiCl_2$ was first directly added to the $AlCl_3$-EMIM electrolyte. After 24 hours of stirring, a bright orange suspension was obtained, as shown in Figure 4(a). Leaving the electrolyte unstirred for 24 hours forced the undissolved particles to settle at the bottom of the beaker, as shown in Figure 4(b). These observations suggest low solubility of $NiCl_2$ in acidic choloraluminate electrolyte, in agreement with previous reports [35].

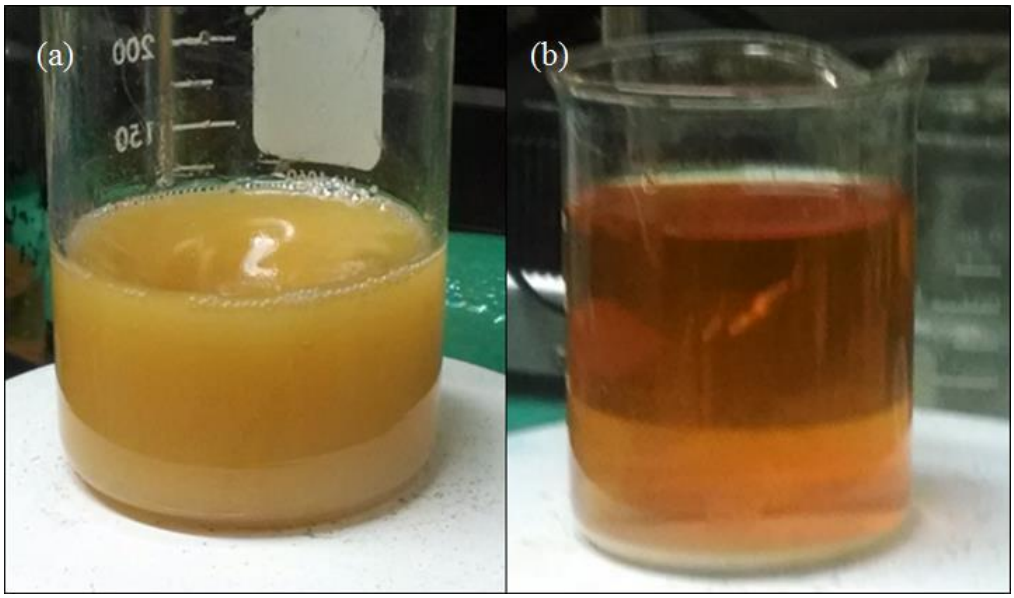

Figure 4. (a) Photograph of bright orange $AlCl_3$-EMIM-$NiCl_2$ suspension; (b) $AlCl_3$-EMIM-$NiCl_2$ with undissolved $NiCl_2$ at the bottom.

Next, the effect of temperature on the dissolution behavior of $NiCl_2$ in the electrolyte was studied. It was reported that elevated temperature enhanced $NiCl_2$ dissolution in $AlCl_3$-BPC [7]. The electrolyte was carefully elevated to 80°C using a heating mantle and stirred for 24 hours, as shown in Figure 5. The resultant electrolyte appeared to be one shade darker but still had undissolved particles suspended indicating poor dissolution of $NiCl_2$.

Figure 5. Photograph of $AlCl_3$-EMIM-$NiCl_2$ being heated and stirred in heating mantle at 80°C.

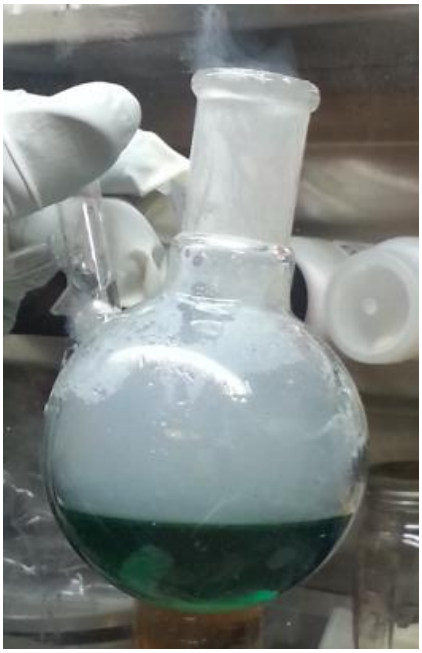

Figure 6. Photograph of basic $NiCl_2$-EMIM-$AlCl_3$ solution.

It was found that $NiCl_2$ was readily dissolvable in basic $AlCl_3$-EMIM electrolyte, similar to previous study [42]. Desired amount of $NiCl_2$ was first added to EMIM. $AlCl_3$ was then slowly introduced in the beaker making sure that the $AlCl_3$ falls on the $NiCl_2$. $AlCl_3$ immediately reacts with EMIM leading

to an acid base reaction. This reaction is exothermic, accompanied by the release of white fumes. When the molar fraction of $AlCl_3$ is less than 0.5, the solution formed was basic which favors the dissolution of $NiCl_2$. A dark green solution was observed, as depicted in Figure 6. Increasing $NiCl_2$ concentration from 0.026 to 0.1 M changes the color of the solution from dark green to blue.

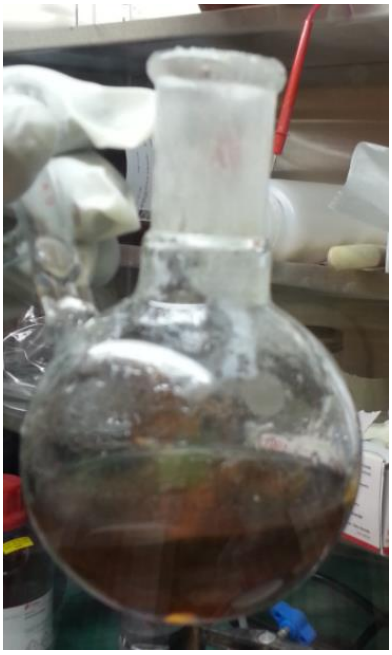

Figure 7. Photograph of acidic $AlCl_3$-EMIM-$NiCl_2$ solution.

As soon as the molar fraction of $AlCl_3$ reaches 0.5, the solution turns brown (Figure 7), indicating a shift from basic to acidic solution. Further addition of $AlCl_3$ was performed to shift the reduction potential of Al to support its deposition. It was noticed that $AlCl_3$ was easily dissolved beyond 1:1 molar ratio of $AlCl_3$: EMIM but could not reach 2:1 as excess $AlCl_3$ precipitated without dissolution. This can be understood by the fact that Ni^{2+} ions consume some of the EMIM anions making less available reactive anions for Al^{3+} cations. For this reason the molarity of the electrolyte was limited to 1.5:1 for all experiments. The resultant solution was a clear brown solution having Al and Ni ions.

Further purification of the $AlCl_3$-EMIM-$NiCl_2$ electrolyte was attempted by dipping a pure Al plate and stirring the solution for 5 days. The solution changed its color to light green as shown in Figure 8(a). An interesting characteristic which was noted was the presence of black powder in the solution after the

purification process. The black powder starts to form as soon as Al comes in contact with the solution and clings to Al as seen in Figure 8(b).

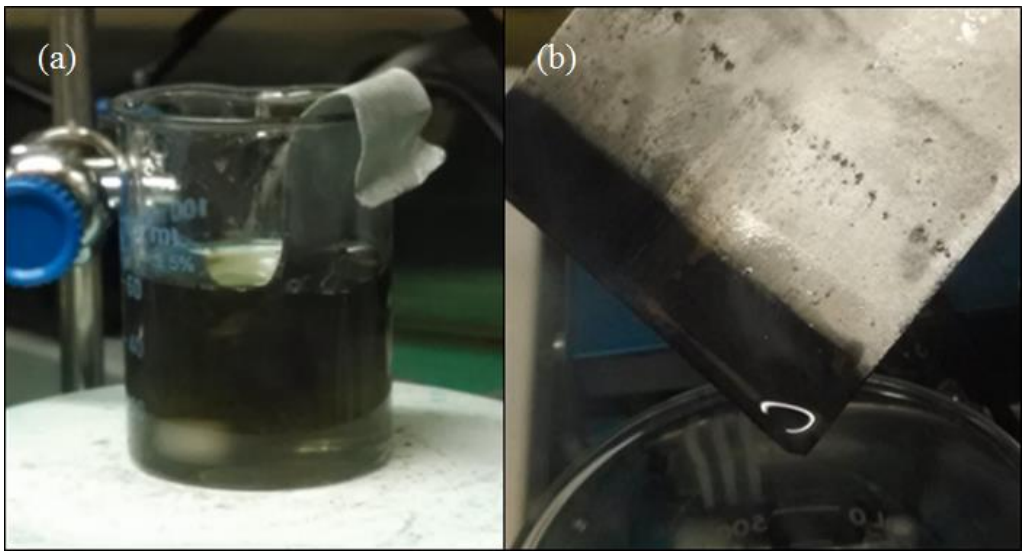

Figure 8. (a) Purifying $AlCl_3$-EMIM-$NiCl_2$ with Al plate; (b) black powder on Al plate.

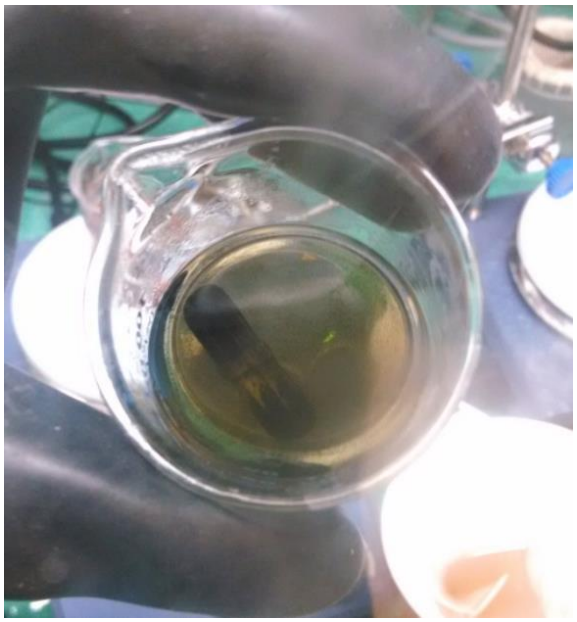

Figure 9. Photograph of black powder magnetically accumulated on stir rod.

The solution was filtered using a 90 mm diameter filter paper which separated the black powder from the solution. The black powder had a hint of green color as seen on the filter papers which suggests it

being an oxide of Ni. These powders also displayed a magnetic nature since they adhered to the stir rod as seen in Figure 9. This process led to a solution with poor ED characteristics. To avoid this, the electrolytes prepared for this research were used without purification with Al plate.

For the purpose of this research, 1.5:1 molar ratio $AlCl_3$-EMIM, 1.5:1 molar ratio $AlCl_3$-EMIM containing 0.024 mol l^{-1} $NiCl_2$, 1.5:1 molar ratio $AlCl_3$-EMIM containing 0.026 mol l^{-1} $NiCl_2$ and 1.5:1 molar ratio $AlCl_3$-EMIM containing 0.1 mol l^{-1} $NiCl_2$ were synthesized following the above stated method. All solutions appeared clear and were kept under inert environment.

2.4.2 Electrochemical Characteristics of the Electrolytes

To better understand the characteristics of the synthesized electrolytes, cyclic voltammograms were obtained in a three electrode configuration cell. In conventional cyclic voltammetry, a voltage sweep is generally applied on the WE from a positive to a negative potential within the electrochemical window of the electrolyte and the corresponding current density is recorded. The ions in the electrolyte undergo oxidation and reduction on the WE resulting in stripping and deposition of the metal respectively. These redox reactions generate current peaks in the voltammogram that can be effectively used to optimize the ED by selecting desired currents or voltages.

A voltage sweep starting from 2 V vs Al/Al^{3+} to -0.5 V and reversed back to 2 V was applied to determine the oxidation and reduction peaks suggesting dissolution and deposition of the respective metals or alloys respectively. It should be noted here that all voltages mentioned in this work are measured vs Al/Al^{3+}, for convenience only voltage value is written. The cyclic voltammograms acquired for electrolytes of different molarities revealed the potentials for the ED of Al, Ni and Al-Ni alloy which could be then used to optimize the constant potential or potential waveform to achieve desired metal contents. Cyclic voltammetry was performed on inert W electrode at room temperature to reveal the reduction and oxidation potentials. The peak shapes in the voltammograms are consistent with those illustrated for $AlCl_3$-EMIM and $AlCL_3$-EMIM-$NiCl_2$ [7, 24, 29, 35, 43-47]. The voltammogram in $AlCl_3$-EMIM is depicted in Figure 10(a).

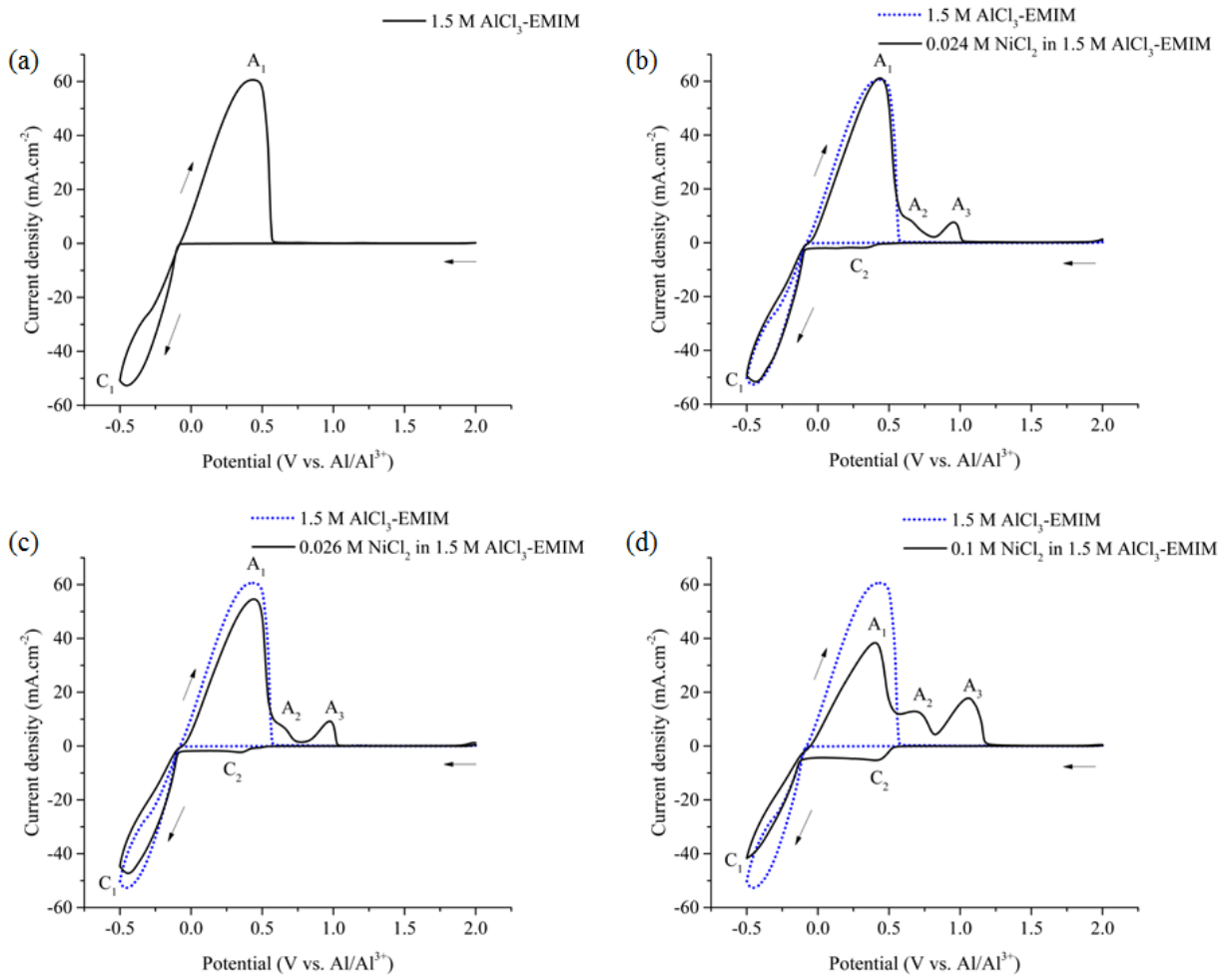

Figure 10. A series of cyclic voltammograms on W electrodes measured with scan rate of 20 mV/s with a step size of 2 mV: (a) $AlCl_3$-EMIM; (b) $AlCl_3$-EMIM compared with $AlCl_3$-EMIM containing 0.024 mol l^{-1} $NiCl_2$; (c) $AlCl_3$-EMIM compared with $AlCl_3$-EMIM containing 0.026 mol l^{-1} $NiCl_2$; (d) $AlCl_3$-EMIM compared with $AlCl_3$-EMIM containing 0.1 mol l^{-1} $NiCl_2$.

A reduction wave C_1 and an oxidation peak A_1 with a peak potential at 0.44 V is observed which is attributed to the bulk deposition and bulk stripping of Al respectively. Al reduction started at -130 mV vs Al/Al^{3+} revealing the need of a relatively large nucleation overpotential [24]. Voltammograms obtained on W electrode in $AlCl_3$-EMIM with 0.024 mol l^{-1} $NiCl_2$, $AlCl_3$-EMIM with 0.026 mol l^{-1} $NiCl_2$ and $AlCl_3$-EMIM with 0.1 mol l^{-1} $NiCl_2$ melts in contrast to $AlCl_3$-EMIM without $NiCl_2$ are shown in Figure 10(b-d). A close examination of these figures exposes reduction peaks C_2 with the peak potentials around 0.4 V for electrolytes containing $NiCl_2$ which is attributed to the deposition of bulk Ni, as confirmed by EDS analysis.

This reduction follows the reaction in Equation 2.2. This association also becomes evident since this peak is missing from the voltammogram of the melt without $NiCl_2$. Consequently, minor oxidation peaks A_3 with potentials ranging from 0.9 to 1.2 V corresponds to the relative stripping of bulk Ni, which correlates with the C_3 peak [29].

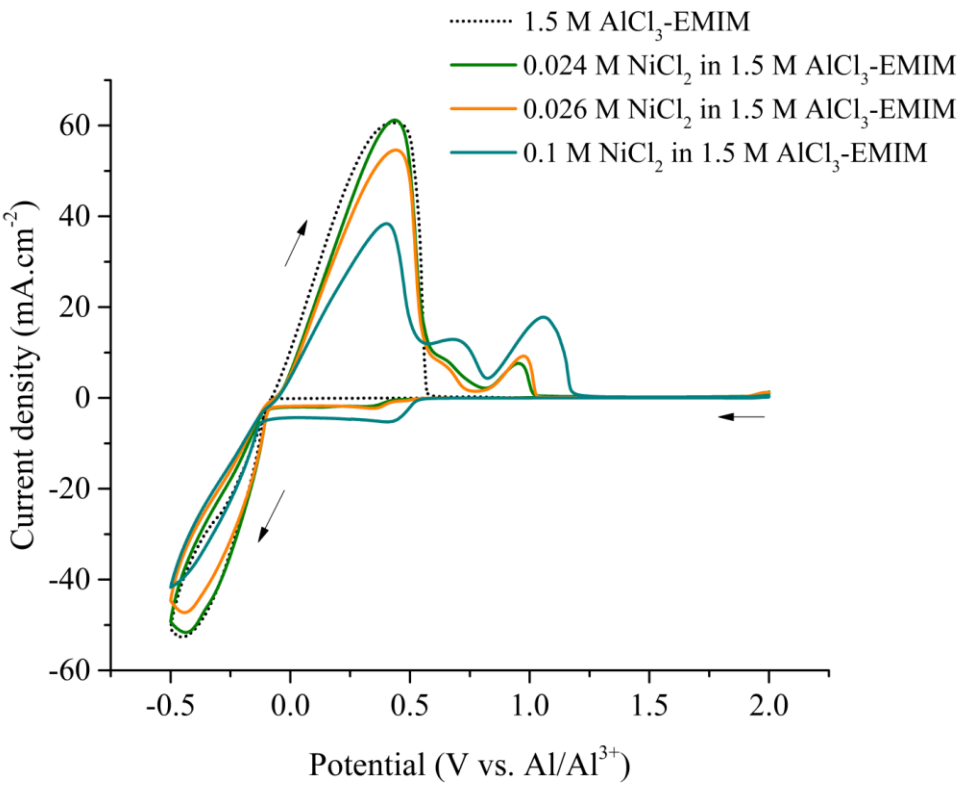

Figure 11. A comparison of cyclic voltammograms on W electrodes in $AlCl_3$-EMIM, $AlCl_3$-EMIM containing 0.024 mol l^{-1} $NiCl_2$, $AlCl_3$-EMIM containing 0.026 mol l^{-1} $NiCl_2$ and $AlCl_3$-EMIM containing 0.1 mol l^{-1} $NiCl_2$ measured with scan rate of 20 mV/s with a step size of 2 mV.

The constant cathodic peaks ranging from -0.12 to 0.3 V can be attributed to the deposition of intermetallic Al-Ni alloys since this range corresponds to their deposition potential range which is 0.08 to -0.2 V [7]. The counterpart oxidation peaks A_2 are considered as the stripping of the Al-Ni alloy. The stripping potential range of Al-Ni alloys is 0.6 V [29]. These intermetallics are deposited according to the reaction in Equation 3.1. Figure 11 shows the voltammograms of all the melts containing $NiCl_2$ in comparison with the 1.5:1 $AlCl_3$-EMIM melt. It can be clearly stated that the amount of $NiCl_2$ dissolved in

the melt is in direct proportionality with the intensities of C_2, A_2 and A_3 peaks. With more $NiCl_2$ added, a greater concentration of Ni^{2+} ions are available in the electrolyte giving rise to higher reduction and oxidation peaks. On the contrary, Al reduction and oxidation peaks (C_1 and A_1) become less intense. This can be attributed to the decrease in available Al^{3+} ions due to more Ni^{2+} ions initially present in the solution.

Jiang et al. [24] found the presence of an additional reduction and oxidation peak for Al at 0.1 V and 0.4 V respectively on a W electrode in 2:1 molar ratio $AlCl_3$-EMIM molten salt. The stripping of Al at this reduction peak was attributed to the underpotential deposition (UPD) and relative oxidation proven by the Kolb-Gerischer's UPD correlation. The presence of these UPD peaks were said to be visible only if the W substrate went through intensive pretreatment. Due to the small magnitude of these peaks, they were not visible due to the presence of other peaks at the same potentials in 1.5:1 molar ratio $AlCl_3$-EMIM electrolyte.

2.4.3 Effect of Working Electrode

To understand how the working electrode affects the deposition/stripping potentials and current densities of Al and Ni, cyclic voltammograms were also acquired on Cu substrates initiating at 2 V sweeping to the negative direction and reversed at a negative potential of -0.5 V. CV of $AlCl_3$-EMIM was depicted in Figure 12(a). Unlike inert W, Cu is electrochemically active thus an anodic potential vs. the aluminum reference electrode is observed until the first reduction peak is created. This potential can be related to the constant dissolution of Cu in the electrolyte [41]. The peak C_1 on the scan attributed to the reduction of Al reveals that the deposition of Al starts at -0.2 V, which deviated slightly from the C_1 on W. Consequently, the peak A_1 corresponds to the oxidation of bulk Al where Al is completely stripped away from the substrate. The reduction peak C_3 at 0.5 V conforms to the deposition of Cu as it lies in proximity of the standard reduction potential of Cu shown in Table 1. Cu undergoes oxidation represented by the A_3 peak at 1.5 V since the Cu electrode etched away at this potential. Minor oxidation and reduction peaks (A_2 and C_2) can also be noticed in the voltammogram in Figure 12(a). These peaks are related to the underpotential stripping and deposition of Al on the Cu substrate.

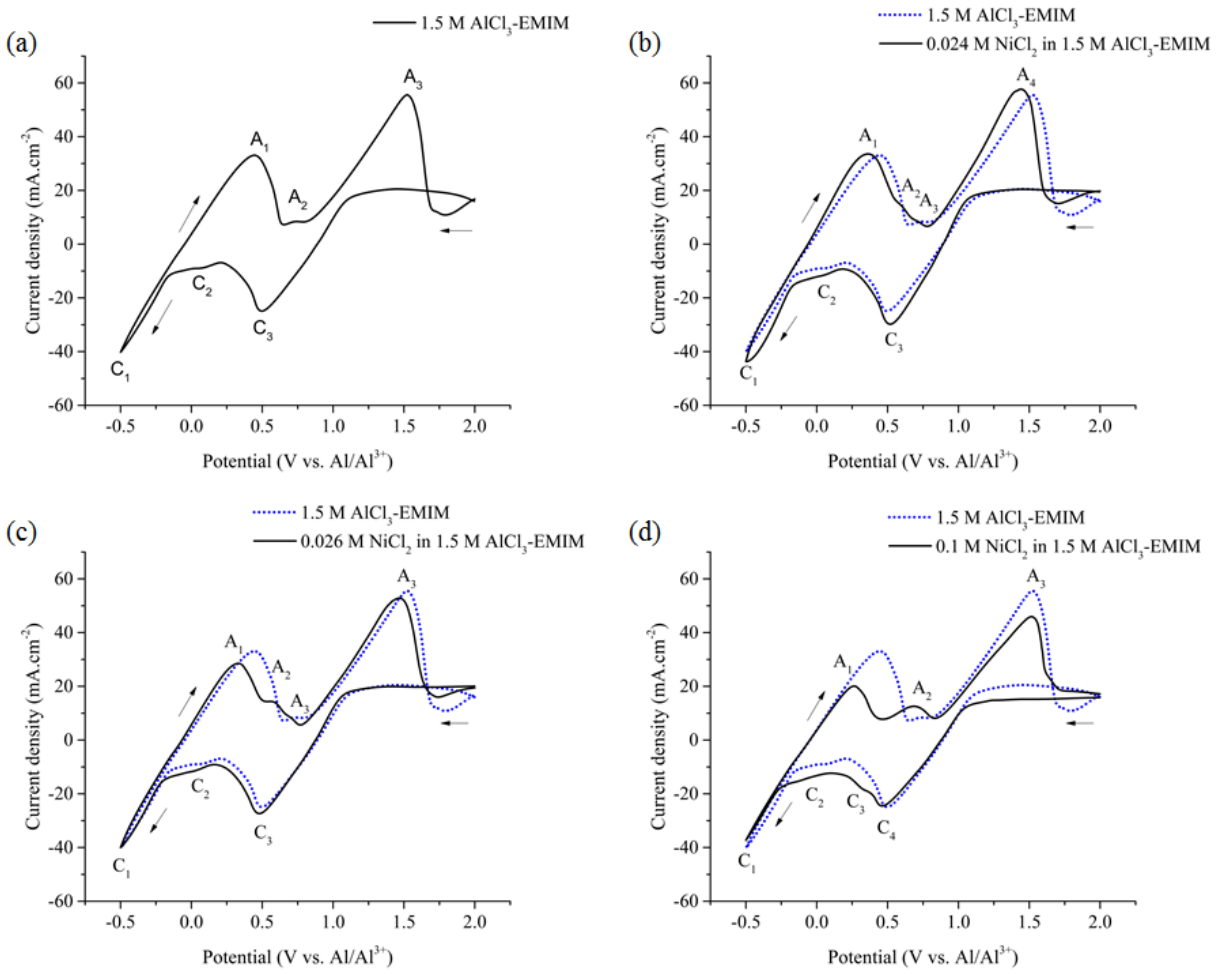

Figure 12. A series of cyclic voltammograms on Cu electrodes measured with scan rate of 20 mV/s with a step size of 2 mV: (a) $AlCl_3$-EMIM; (b) $AlCl_3$-EMIM compared with $AlCl_3$-EMIM containing 0.024 mol l^{-1} $NiCl_2$; (c) $AlCl_3$-EMIM compared with $AlCl_3$-EMIM containing 0.026 mol l^{-1} $NiCl_2$; (d) $AlCl_3$-EMIM compared with $AlCl_3$-EMIM containing 0.1 mol l^{-1} $NiCl_2$.

Voltammograms recorded in $AlCl_3$-EMIM with 0.024 mol l^{-1} $NiCl_2$, $AlCl_3$-EMIM with 0.026 mol l^{-1} $NiCl_2$ and $AlCl_3$-EMIM with 0.1 mol l^{-1} $NiCl_2$ in comparison with $AlCl_3$-EMIM without $NiCl_2$ are shown in Figure 13(b-d). An additional Ni oxidation peak A_3 at around 0.7 V shows up and a slight cathodic shift in peaks C_2 is observed in Figure 12(b and c). The increase in intensity of the reduction peaks reveal the reduction potential of Al-Ni intermetallics and bulk Ni around 0 and 0.3 V respectively. The peak A_3 corresponds to the relative removal of the Al-Ni deposit.

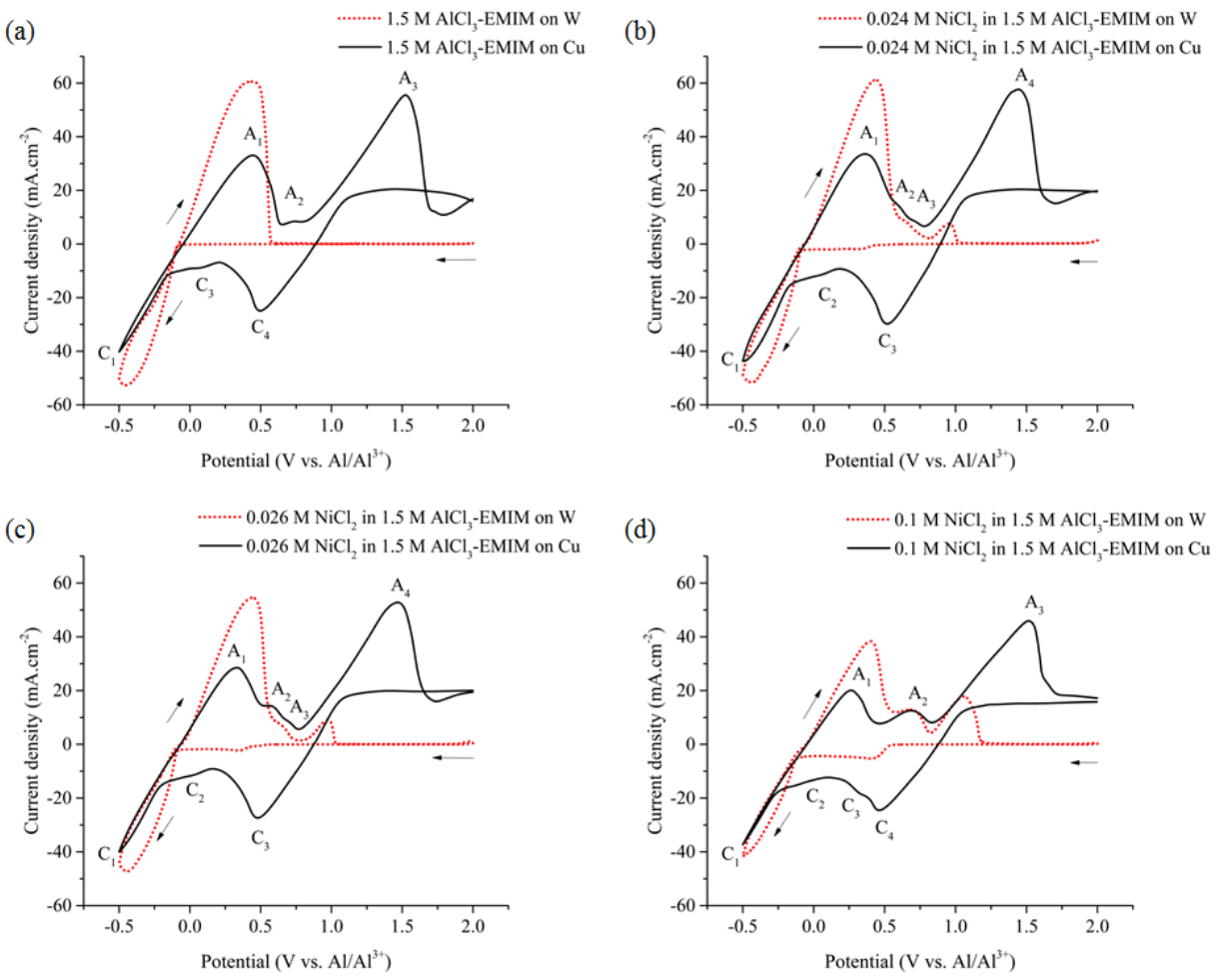

Figure 13. A series of cyclic voltammograms measured with scan rate of 20 mV/s with a step size of 2 mV: (a) $AlCl_3$-EMIM on W vs. Cu; (b) $AlCl_3$-EMIM containing 0.024 mol l^{-1} $NiCl_2$ on W vs. Cu; (c) $AlCl_3$-EMIM containing 0.026 mol l^{-1} $NiCl_2$ on W vs. Cu; (d) $AlCl_3$-EMIM containing 0.1 mol l^{-1} $NiCl_2$ on W vs. Cu.

These arguments can be supported by a close examination of the voltammograms recorded on Cu in comparison with W for these electrolytes, as shown in Fig 13(a-d). It can be noticed in Figure 13(b-d) that the Al-Ni stripping peaks on Cu are at the same potential as those on W. It is also noticed that the oxidation of bulk Ni peak around 1 V is hidden under the bigger A_3 peak on the Cu voltammogram. The role of C_3 also becomes clearer in Figure 13(d) as it coincides with the potential for bulk Ni deposition on the W counter electrode. Figure 14 depicts the voltammograms of all the melts containing $NiCl_2$ in comparison with the 1.5:1 $AlCl_3$-EMIM melt on Cu substrate. It can be clearly stated that the Ni and Al-Ni

peaks increase with the increasing amount of $NiCl_2$ dissolved in the melt. The increase in the Ni peaks are counterbalanced by the evident decrease in the Al peaks owing to the less dissolution of $AlCl_3$ in the electrolyte.

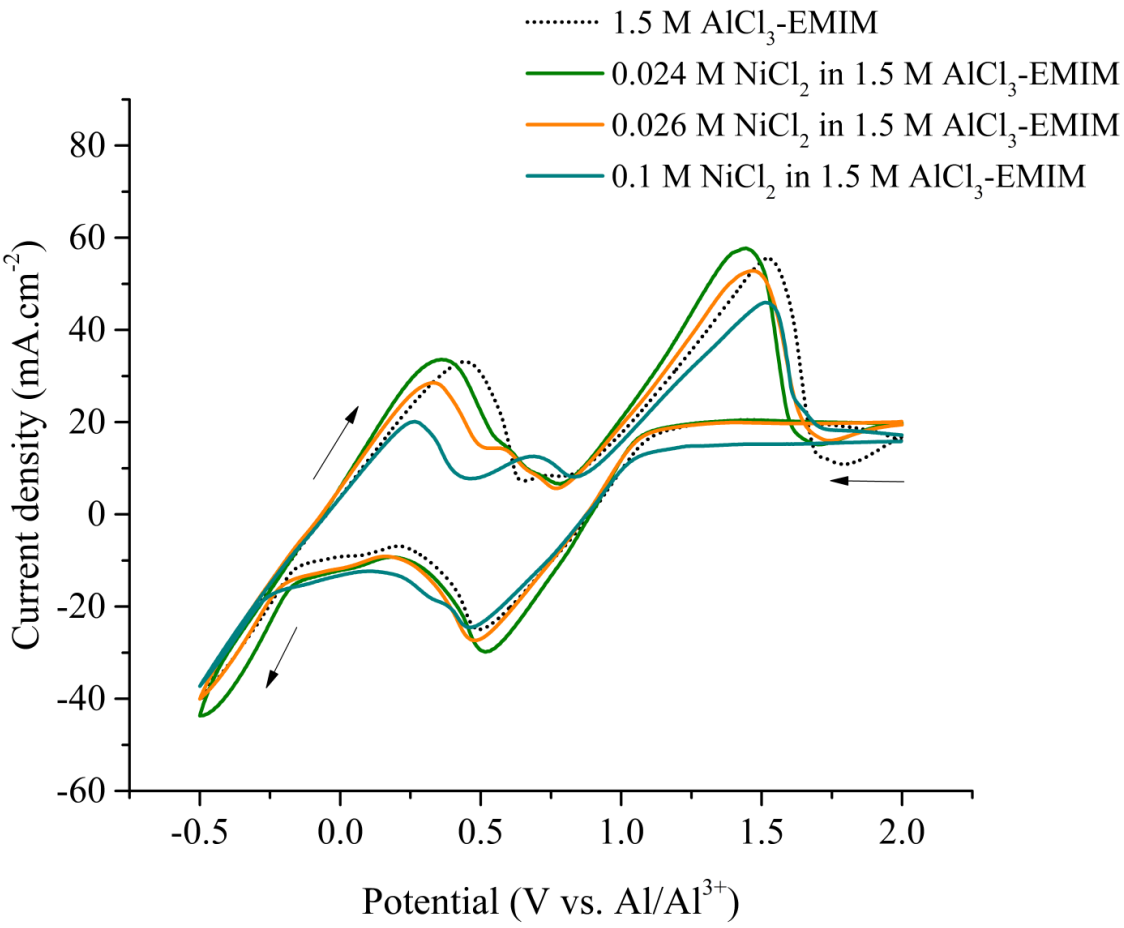

Figure 14. A comparison of cyclic voltammograms on Cu electrodes in $AlCl_3$-EMIM, $AlCl_3$-EMIM containing 0.024 mol l^{-1} $NiCl_2$, $AlCl_3$-EMIM containing 0.026 mol l^{-1} $NiCl_2$ and $AlCl_3$-EMIM containing 0.1 mol l^{-1} $NiCl_2$ measured with scan rate of 20 mV/s with a step size of 2 mV.

Table 1. Selected standard reduction potentials.

Oxidizing Agent	Reducing Agent	Reduction Potential/ V
$Al^{3+} + 3e^-$	Al	-1.66
$Cu^{2+} + 2e^-$	Cu	0.34
$Ni^{2+} + 2e^-$	Ni	-0.26

2.5 Conclusions

From the present study on the synthesis and electrochemical properties of the selected electrolyte system, the following conclusions can be drawn,

1. $AlCl_3$-EMIM-$NiCl_2$ electrolyte of desired molarities was successfully synthesized. Increasing the temperature did not aid the dissolution of $NiCl_2$ in the acidic electrolyte. Dissolution of $NiCl_2$ was favored in basic $AlCl_3$-EMIM molten salt at room temperature.
2. Cyclic voltammograms of the electrolytes on W electrode reveal clear oxidation and reduction peaks for Al, Ni and Al-Ni. Al deposition takes place at potentials more negative to -0.13 V while Ni and its alloy gets deposited ranging from 0 to 0.4 V. The current density of Ni oxidation and reduction peaks varies proportional to the amount of $NiCl_2$ dissolved in the $AlCl_3$-EMIM electrolyte. Al oxidation and reduction peaks show lesser peak potentials with increased Ni content owing to lesser number of Al^{3+} ions present in the melt.
3. The use of an electrochemically active Cu working electrode shows a significant effect on the voltammograms obtained for the same electrolytes. Cu gets dissolved in the electrolyte in the forward scan range of 1 to 2 V. Additional reduction and oxidation peak of Cu is observed at 0.5 and 1.5 V respectively in the voltammetry scan. Underpotential reduction peaks and relative oxidation peaks of Al are also observed with the use of Cu electrode. Unlike W, Cu electrode is highly reactive. The deposition and stripping potentials of Al, Ni and intermetallics does not change using Cu substrate.

CHAPTER 3: ELECTRODEPOSITION OF Al-Ni ALLOYS AND BILAYERS

3.1 Background

Elctrodeposition (ED) of Al-Ni alloys in chloroaluminate electrolytes have been researched by several groups in pursuit of optimizing their mechanical properties and microstructure. A brief comparative study of a few important research works is described next.

3.1.1 Electrodeposition of Al-Ni Alloys in Chloroaluminate Melts

During the ED of Al and Ni, Ni-Al reduction takes place according to the following reaction [29]

$$xNi^{2+} + 4(1-x)Al_2Cl_7^- + (3-x)e^- \leftrightarrow Ni_xAl_{1-x} + 7(1-x)AlCl_4^- \quad (3.1)$$

where x ($0 < x < 1$) represents the molar fraction of Ni in Ni_xAl_{1-x} alloy. Ali et al. [7] deposited Al-Ni intermetallic compounds (mainly Ni_3Al) using potential control, current control and pulse current control in $AlCl_3$-BPC-$NiCl_2$ electrolyte at room temperature. Pure Ni was deposited at potentials greater than 0 V (0.3 to 0.4 V) while a mixture of Ni, Al and Ni_3Al was obtained at potentials from -0.2 to -0.5 V or at current densities of -20 to -35 A m^{-2}. Intermetallics and elemental Ni and Al co-deposited when this limit was exceeded. Ueda et al. [46] performed ED of Al-Cr-Ni in 2:1 molar ratio $AlCl_3$-EMIM with $NiCl_2$ and $CrCl_2$ at 338 K using constant potential control and pulse potential control producing 9 at.% and 20-27 at.% Ni respectively. In constant potential deposition, 20 C cm^{-2} charge density was used on the working electrode keeping the potential constant at 0 and -0.2 V which yielded Al:Cr:Ni of 90:1:9 and 97:2:1 respectively. This low Ni concentration was enhanced greatly by using pulsed potentials with different frequencies and duty cycle ratios. Pitner et al. [29] deposited Ni and Ni-Al alloys using 2:1 molar ratio $AlCl_3$-EMIM melt. Ni ion was introduced to the electrolyte by electrogenerating Ni wire electrode at 1.40 V at 40°C. This method differs from conventional employment of $NiCl_2$ to produce Ni^{2+} ions in the molten salt. The amount of Al in the deposit was found to be linearly dependent on the applied potential and

inversely proportional to Ni content. It was also deduced that the composition of the deposited alloy was dependent upon the charge before 60 mC of charge had been generated. Another commonly used system for ED of Al-Ni was researched by Moffat [6] on a W substrate in inorganic $AlCl_3$-NaCl molten salt consisting of 0.17 mol L^{-1} [Ni^{2+}]. Well adherent and dense deposits were obtained at voltages beyond 0.7 V. Consequently, $Ni_{1-x}Al_x$ alloys were deposited at potentials lesser than 0.6 V while pure Ni was obtained around 0.035 V vs. Al/Al^{3+}.

The deposition of a single phase Al-Ni intermetallic compound was found to be much more effective and convenient using the pulse current controlled electrolysis by Ali et al. [7] in $AlCl_3$-BPC-$NiCl_2$. A single phase fcc structure was observed by Pitner et al. [29] in Al-15 at.% Ni deposits produced at 0.3 V in $AlCl_3$-EMIM electrolyte. These authors also found deposits produced at 0 V and lower potentials are fine magnetic black powders with a dendrite structure. XRD study of these powder deposit indicated the presence of fcc and amorphous phase. In $AlCl_3$-NaCl system, Moffat [6] noticed that the deposited Al-Ni alloys are dense and adherent with nodular structures. Any increase in the overpotential voltage drastically affected the microstructure. A change from nodular to dendritic to powdery structure was observed as potential increases.

Despite the limited studies on ED of Al-Ni alloys as summarized above, a systematic understanding of the effects of deposition parameter on alloy composition and microstructure of Al-Ni from organic ionic liquid electrolyte is still missing. The goal of this chapter is to provide a detailed investigation of the ED of Al-Ni in $AlCl_3$-EMIM system using pulse potential control and investigate the effects of deposition parameters such as potential, duty ratio, frequency, deposition time and substrate on the composition and microstructure of the deposited alloys.

3.1.2 Electrodeposition of Multilayered Al/Ni

In addition to Al-Ni alloys, multilayered Al/Ni is an important engineering material as they exhibit self-propagating property with highly exothermic local reaction at the onset of an external ignition. Matsuda et al. [30] fabricated self-propagating Al/Ni flakes by dual source dc sputtering on nylon mesh substrate.

The atomic ratio of the multilayers was kept 1:1. The flakes were found to exhibit exothermic explosive characteristics. XRD analysis revealed the presence of Al and Ni before the spark ignition. On the contrary only NiAl interatomic compounds were observed after the exothermic reaction. These interatomic compounds formed due to the 1:1 atomic ratio of the Al and Ni in the flakes. Kuk et al. [31] studied the effects of Al/Ni ratio in multilayers prepared by dc magnetron sputtering. They observed that AlNi, $AlNi_3$ and Al_3Ni_2 formed after the ignition reaction when the atomic ratio of Al/Ni layers was kept around 1:1, 1:3 and 3:2 respectively. A comparison of the reaction heats of different samples showed an inverse proportionality of Ni atomic ratio and the reaction heats.

To the best of our knowledge, the electrodeposition of Al/Ni multilayers has not been reported before. Successful ED of Al/Ni multilayers will potentially enhance large scale production of these important materials in complex shapes and structure, which might open new doors to future research in smart energy materials. Thus in addition to ED of Al-Ni alloys, the second goal of this chapter is to investigate the prospects of the ED of Al/Ni multilayers in $AlCl_3$-EMIM-$NiCl_2$. The following milestones need to be accomplished,

- ED of pure Al and Ni
- ED of Ni/Al and Al/Ni bilayers
- ED of Al/Ni multilayers

3.2 Experimental Procedures

Al-Ni alloys were electrodeposited using potential control (including constant and pulsed potential) in a three electrode cell. The electrolyte contains 1.5:1 molar ratio of $AlCl_3$-EMIM with 0.024 to 0.1 M $NiCl_2$. The preparation of the electrolyte is described in Chapter 2. In constant potential controlled deposition, a constant potential in the range of -0.5 to 1.5 V was used, as shown in Fig. 15(a). In pulse potential controlled ED, square wave pulses of high and low voltages were used as depicted in Figure 15(b). The effects of magnitude of potentials, duty cycle ratios, and frequencies on alloy composition and microstructure were examined. Potentioamperometry and Repeating Potentioamperometry modules of Gamry Potentiostat were

utilized for constant and pulse potential deposition respectively. SEM and EDS analysis was performed using Hitachi SU-70 SEM and Hitachi S-800 SEM. FIB images with cross-section of the deposits were obtained using FEI Quanta 200 3D. X-Ray diffraction patterns were obtained using Philips X'Pert X-Ray Diffraction platform.

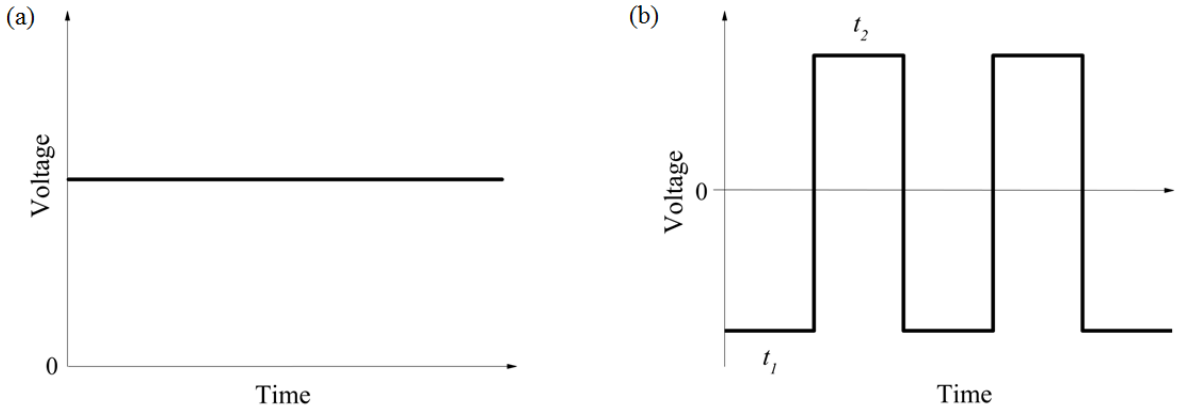

Figure 15. Schematic waveforms of (a) constant potential; (b) pulse potential.

3.3 Results and Discussion

3.3.1 Effect of Deposition Potential on Alloy Composition

The selection of the potentials for Al-Ni deposition was based on the electrochemical properties of the electrolytes in section 2.4.2 and 2.4.3. From chapter 2, the cyclic voltammograms reveal the potentials and respective current densities for the reduction and oxidation of Al and Ni in each melt. The negative potential deposited Al while the positive potential was responsible for the deposition of Al-Ni or bulk Ni. In both cases, the potential ranging from 0.15 to 0.4 V of the positive cycle of the pulse also stripped Al since this range also corresponds to the anodic oxidation of Al. Table 2 lists the samples prepared with respect to experimental parameters and their composition as a function of potential waveform applied.

The concentration of Al and Ni in the alloy was found to be critically dependent on the amount of $NiCl_2$ in the electrolyte, potential, duty cycle ratio and frequency. Samples 3 and 5 were deposited using the same potential, duty ratio and frequency in $AlCl_3$-EMIM containing 0.026 M and 0.1 M $NiCl_2$

respectively. It was observed that Ni concentration increased from 2 to 6 at.% by increasing the $NiCl_2$ dissolved in the melt. The increased Ni content corresponds to the increased partial current densities of reduction peaks C_2 and C_3 in Figure 12(c) and (d). On the other hand, the Al deposition peaks C_1 in Figure 12(c) and (d) become less intense with the increased [$NiCl_2$] thus decreasing Al concentration in the alloy. This increment of Ni concentration with increasing [$NiCl_2$] in the electrolyte is similar to previous studies [29]. However, this increment is not linear. For example, from sample 3 to 5, increasing [$NiCl_2$] from 0.026 to 0.1 M will increase Ni concentration from 2 at.% to 6 at.%. Hence, the concentration of Ni in the alloy increases nonlinearly with the increase of [$NiCl_2$] in the melt. This non-linear proportionality with a much greater deviation can also be observed when comparing samples 1 and 6.

Table 2. Electrodeposition parameters and composition of deposits.

Sample	Amount of $NiCl_2$ in $AlCl_3$-EMIM (M)	Substrate	Negative Potential (V)	Positive Potential (V)	Duty cycle ratio of negative to positive	Frequency f (Hz)	Deposition time (s)	Concentration (wt.%)		Concentration (at.%)	
								Al	Ni	Al	Ni
1	0.024	Cu	-0.3	0.15	9::1	1	3600	94.3	5.7	97.3	2.7
2	0.026	Cu	-0.5	0.4	4::1	1	3600	95.8	4.2	98.1	1.9
3	0.026	Cu	-0.3	0.15	1::1	1	7200	95.7	4.3	98	2
4	0.026	Cu	-0.3	0.15	1::1	0.5	7200	90.4	9.6	95.3	4.7
5	0.1	Cu	-0.3	0.15	1::1	1	7200	87.8	12.2	94	6
6	0.1	Cu	-0.3	0.15	9::1	1	7200	94.1	5.9	97.2	2.8
7	0.1	Electrodeposited Cu	-0.3	0.15	1::1	1	3600	68.2	31.8	82.3	17.7
8	0.026	Electrodeposited Cu	-0.3		-	-	150	Pure Al			
9	0.026	Cu	0.4		-	-	375	Pure Ni			

Sample 5 and 6 with duty ratios 1:1 and 9:1 respectively were deposited in $AlCl_3$-EMIM containing 0.1 M $NiCl_2$ using the same potentials. It was observed that the Al and Ni contents increased with increasing the time of positive and negative cycle of the pulse respectively. In sample 5, the 9:1 ratio potential pulse spends most of the time in the negative cycle at -0.3 V responsible for depositing Al while the positive pulse which is just $1/10^{th}$ of the total cycle, decreases the time for the deposition of Ni and stripping of Al. In sample 6, the 1:1 duty ratio enables both negative and positive cycles to deposit Al and Ni respectively for equal amounts of time thus increasing the Ni content compared to sample 5. The relationship of the duty cycle ratio to the Al and Ni concentrations is, however, not linear. Ideally, if 9:1 duty cycle produces 2.8 at.% Ni with the balance being Al, a 1:1 duty cycle waveform with the same positive and negative potentials should produce 12.6 at.% Ni. However, instead we observe 6 at.% Ni, which is almost half of the expected

value. At Ni deposition potential, Al stripping peak of a current density of 18 $mA.cm^{-2}$ is also present. Thus in 1:1 duty ratio, Al also gets stripped away more, which can be one of the reasons to explain the less than expected Ni concentration.

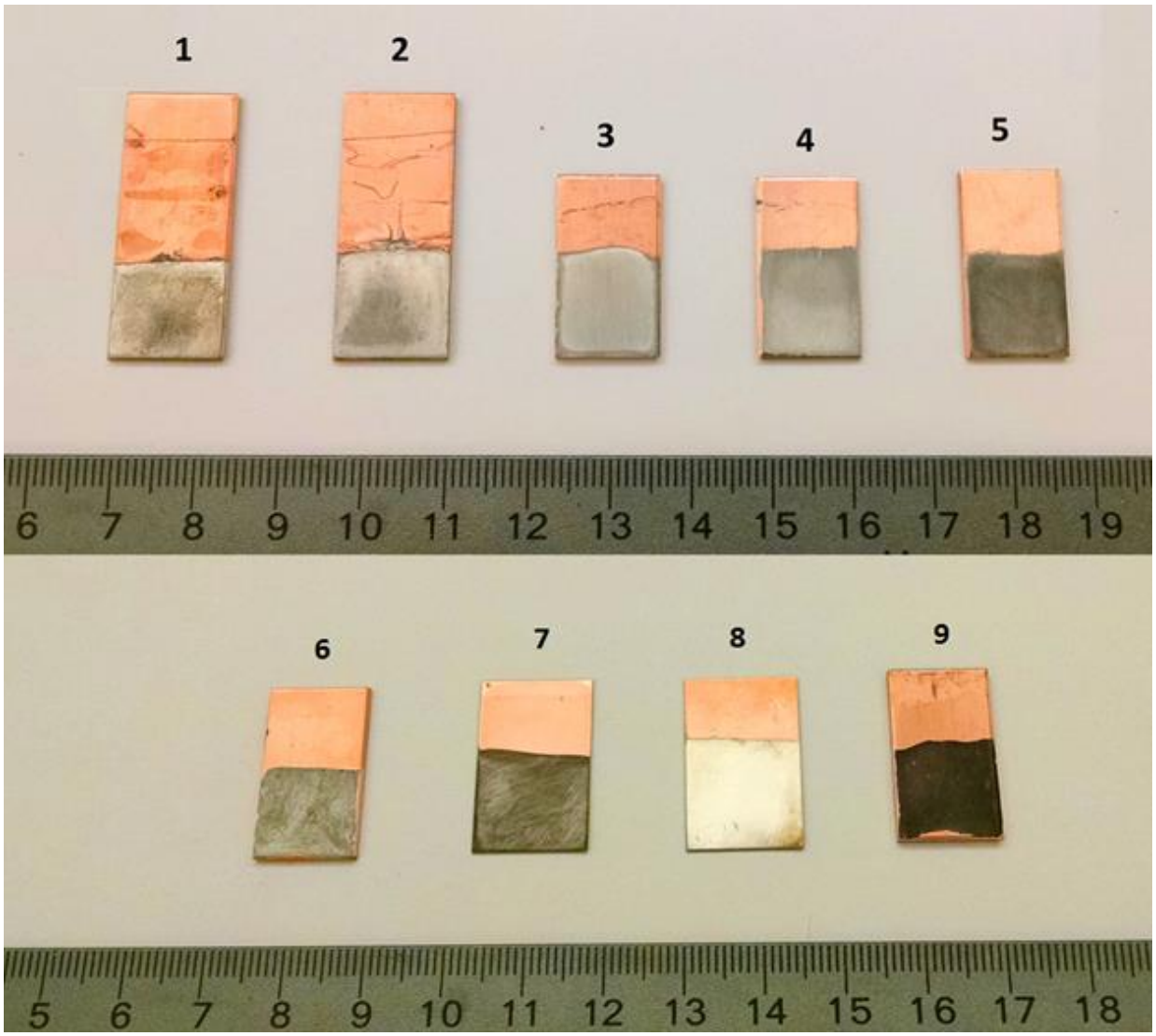

Figure 16. Photograph of electrodeposited samples.

The effect of frequency on the Al-Ni composition can be analyzed using samples 3 and 4 deposited with frequencies 1 and 0.5 Hz with the same electrolyte, potential and duty ratio. Decreasing the frequency by half resulted in almost double the amount of Ni in the deposited alloy. With a frequency of 1 and 0.5 Hz, the deposition of Al and Ni takes place for 0.5 s and 1 s in each cycle respectively. As previously

described, Ni deposition occurs via three dimensional progressive nucleation following a current time transient with a very high slope followed by a diffusion controlled nuclei growth [29]. With more time for each cycle in the 0.5 Hz frequency, the current transient which increases steeply with time during the nucleation phase draws more current in 1 s as compared to that drawn in 2 cycles of 0.5 s in 1 Hz frequency. This increased current density on the Ni deposition cycle results in the increased Ni content.

The surface roughness of the Cu substrate also played a vital role on the composition of the Al-Ni alloy. A very smooth electrodeposited Cu substrate (Kocour) was tested for this purpose. Sample 7 was deposited on electrodeposited Cu with the same potential, frequency, duty ratio and electrolyte as sample 5. Ni concentration was found to increase from 6 to 17.7 at.%. The electrodeposited Cu substrate provides a much smoother surface with nano scale roughness which might favor metal nucleation. On rough Cu substrate, loose black powdered Ni sticks to the substrate due to its magnetic nature. Wiping the sample removes these powdered Ni. This black powder was notably less on the smoother Cu substrate. EDS analysis also revealed that the samples with darker color usually indicated higher Ni content, as shown in both Table 2 and Figure 16.

3.3.2 Scanning Electron Microscopy (SEM) – Surface Morphology

Visual appearance of the deposited samples can be seen in Figure 16. All Al-Ni deposits are compact and well adherent to the substrate. Pure Al deposit (sample 8) has a mirror like silver color. Pure Ni deposit (sample 9) has a dull black color. All other Al-Ni samples have colors in between pure Al and Ni and the darkness increases with Ni content.

SEM image of sample 1 in Figure 17(a) shows dense nodular like structures consistent with previous work of electrodeposited Al-Ni alloys [7]. Sample 2 shows a columnar surface morphology with widely spread nodules, as shown in Figure 17(b). A close examination on the inset image of Figure 17(b) shows the presence of smaller nodules in the range of 10-15 μm with a cauliflower like appearance which is also observed in previous work [29].

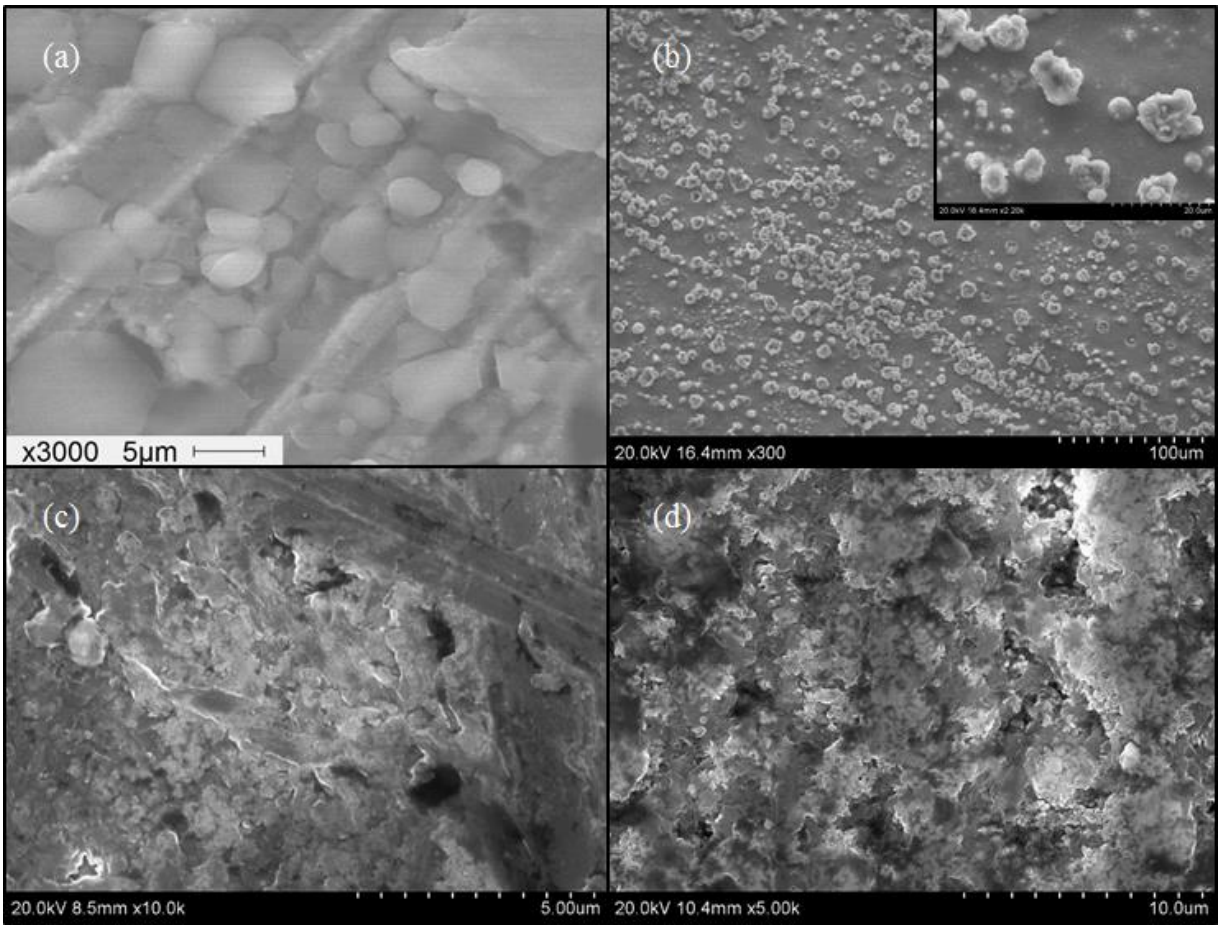

Figure 17. SEM images of (a) sample 1; (b) sample 2; (c) sample 3; (d) sample 5.

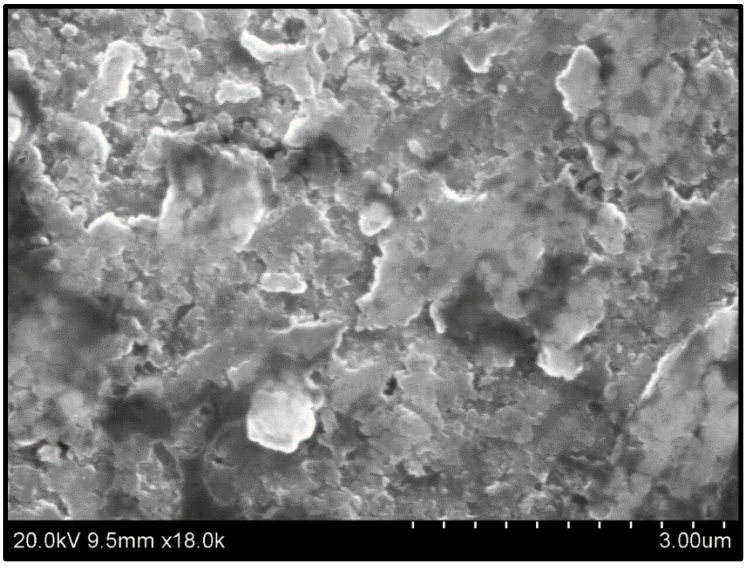

Figure 18. SEM image of sample 7.

The cauliflower structure appears due to higher deposition rate with the increase of potential [3, 39]. Sample 3 and 5 show coarse flake like structures in Figure 17(c) and (d). The increase in the thickness of the deposits makes the surface of Al-Ni rougher [7]. This hypothesis suggests that since these samples were deposited for 2 hours, the columnar structure disappeared resulting in rough flake like structures.

Another factor that might play a role in inflicting the flake structures in the deposits is the surface roughness of the Cu substrate used for the deposition. To test this and the effect of deposit thickness, hypothesized above, sample 7 was deposited on the smooth Cu substrate using the same parameters as sample 5. The microstructure of the alloy is depicted in Figure 18 which shows the same flake structures. So this structure is independent of the surface roughness. Also, similar to samples 1 and 2, sample 7 showed columnar structures, was deposited for 1 hour but it still displayed the same microstructure as that for a 2 hour deposit on sample 5.

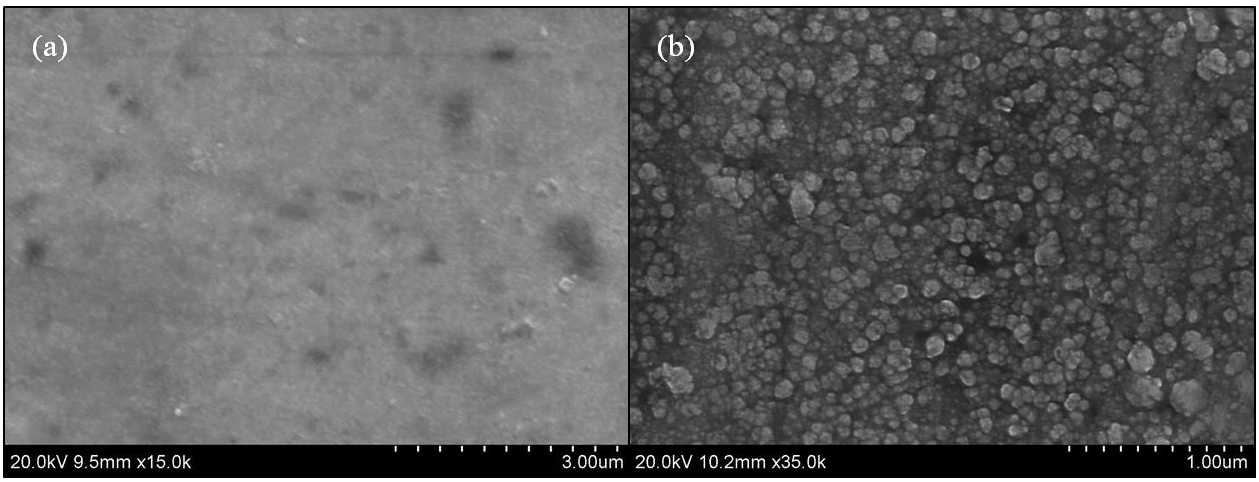

Figure 19. SEM images of (a) pure Al deposit at -0.3 V in 1.5:1 M $AlCl_3$-EMIM containing 0.026 M $NiCl_2$; (b) pure Ni deposit at 0.4 V in 1.5:1 M $AlCl_3$-EMIM containing 0.1 M $NiCl_2$.

Sample 3, 5 and 7 show the same flake structure and were all deposited using the same potential, duty cycle and frequency. Also this structure seems to be independent of the molarity of $NiCl_2$ in the melt since it was different for sample 3. The formation of these flakes is not related to the potential used since sample 1 uses the same potential but formed columnar structure. At the same time, it is not due to the frequency since samples 1 and 2 have the same frequency. The only parameter which all of the flake

structured deposits have in common is the duty ratio. These results indicate that the increased time for the Ni deposition and Al stripping in the positive cycle of the pulse is affecting the microstructure. Al deposits generally have nodular morphology but they have also been reported to form flake structures [38]. While Ni deposits have been shown to have columnar cauliflower structures [3]. The flake structures of Al-Ni deposits observed here seem to be a hybrid of the flake Al and cauliflower Ni.

In addition to depositing Al-Ni alloys, pure Al and pure Ni were also deposited on the electrodeposited Cu substrate. Pure Al was deposited at a constant potential of -0.3 V in 1.5:1 M $AlCl_3$ - EMIM containing 0.026 M $NiCl_2$. The SEM image shown in Figure 19(a) reveal the surface morphology of the deposited metal. The deposit shows a very compact and dense deposit with very fine crystallites in the nanometer region similar to previous work [45, 47, 48]. Constant potential deposition at 0.4 V was utilized in 1.5:1 M $AlCl_2$-EMIM containing 0.1 M $NiCl_2$ to obtain pure Ni deposits. Compact and dense deposits with typical nodular cauliflower structures were obtained as illustrated in Figure 19(b) which has been previously observed in Ni deposits in chloroaluminate melts [3, 39].

3.3.3 X-Ray Diffraction (XRD) – Phase Identification

To identify the presence of different compounds, crystal structure and phase, XRD analysis was carried out to XRD pattern obtained on the sample 1 is shown in Figure 20(a).

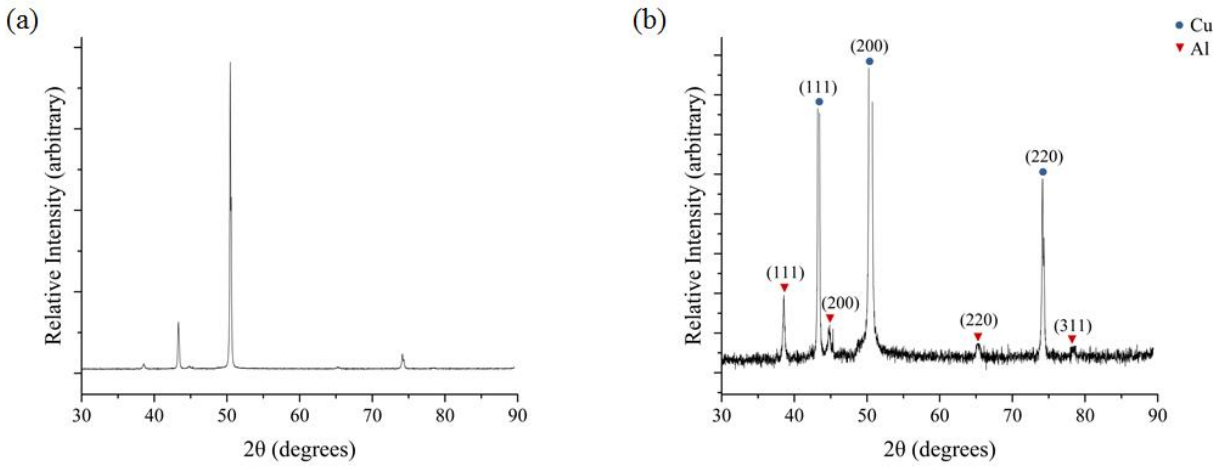

Figure 20. XRD patterns of sample 1 (a) full pattern (b) zoomed in detailed pattern.

Sharp and well defined reflections revealing the presence of crystalline structure is observed for the alloy and the Cu substrate. A close inspection on the pattern in Figure 21(b) indicate FCC Cu diffraction peaks at 2θ = 43.3, 50.5 and 74.2° corresponding to (111), (200) and (220) indices. FCC Al diffraction peaks at 2θ = 38.6, 44.8, 65.4 and 78.6° corresponding to (111), (200), (220) and (311) indices. These peaks represent a single phase supersaturated FCC solid solution of Al-Ni . The pattern does not show diffraction peaks pertaining to pure Ni. Also, Al-Ni intermetallics are not present in the alloy.

3.3.4 Electrodeposition of Al/Ni Bilayers

An attempt to deposit Al/Ni multilayers starts with the deposition of bulk Al and Ni as shown in section 3.3.2. Various constant potentials/currents and pulse potentials were used to test the deposition characteristics of Al/Ni. A test bilayer sample with Ni deposited on electrodeposited Cu with a pulse potential of 0 and 0.78 V for 800 s and Al deposited at a constant -0.3 V for 150 s in $AlCl_3$-EMIM containing 0.026 M $NiCl_2$ was prepared.

The first cycle of the pulse potential waveform for the deposition of Ni was set to 0V. 0.78 V for the second cycle was chosen as the potential where the current becomes zero from voltammogram in Figure 12(c). This type of waveform was selected to promote progressive nucleation of Ni in each cycle as opposed to a constant potential which imparts diffusion controlled growth of Ni nuclei. The Ni deposit appeared to be a dense dull black deposit similar to sample 9 while Al layer deposited on top of that had a uniform mirror like shiny silver deposit. A cross-section of the Ni/Al bilayer was milled using FIB as shown in Figure 21.

The area chosen to mill was first coated with 1 µm Pt protective later. Progressive milling of the sample with decreasing currents as low as 50 pA revealed the presence of Al and Ni layers on electrodeposited Cu substrate. The SEM image in Figure 21 shows a clear color contrast between the darker Al and brighter Ni layers. However, the difference in color contrast between Ni and Cu is not clearly visible since their atomic numbers differ only by 1. The known thickness of the electrodeposited Cu is 1 µm. From

this, the thickness of Ni layer was estimated to be 1 µm while that of Al was 250 nm. The darker region beneath the electrodeposited Cu is the substrate.

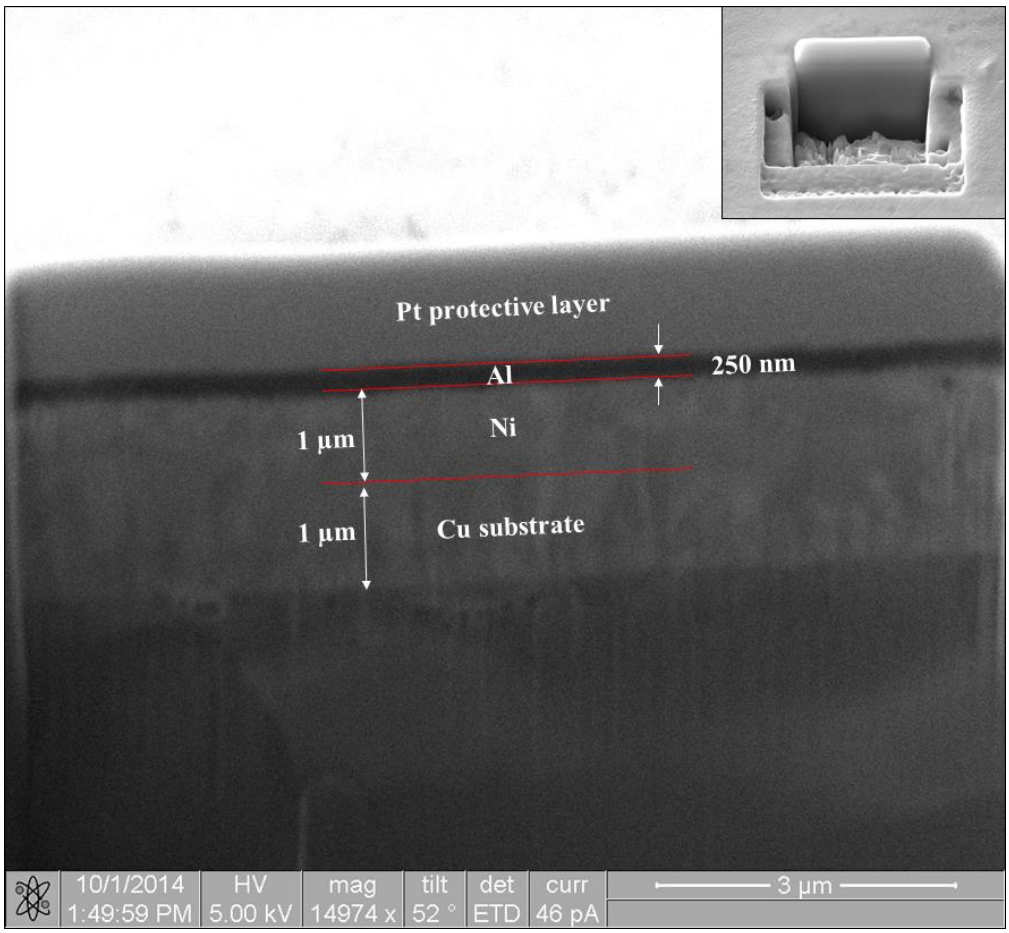

Figure 21. SEM image of a FIB cross-section of Ni/Al bilayer sample.

Upon successfully depositing Al on Ni, the next step was to test the deposition of Ni on Al. For this, Al was deposited on the electrodeposited Cu WE at -0.3 V in $AlCl_3$-EMIM containing 0.026 M $NiCl_2$. A layer of Ni was attempted to deposit on the first Al layer using the same pulse potential waveform used in the previous bilayer. The resultant deposit appeared to have loosely adherent black deposit which upon wiping with kimwipes, revealed scattered black deposits on the Cu substrate. Since the Cu substrate was visible, it clearly indicated that the Al layer deposited before got stripped away. This behavior can be explained by inspecting the cyclic voltammogram of the melt in Figure 12(c). It can be observed that in addition to the presence of the Ni deposition peak at 0 V, this potential also lies in the vicinity of Al

oxidation. Hence, upon electrodepositing Ni on Al, Al also got stripped away. Several constant potential and pulse potential combinations were tried to deposit Ni on Al, but in all the cases, Al stripped away.

Current controlled ED of Ni on Cu was also attempted with current densities ranging from -0.5 to -3.75 mA.cm^{-2}. Compact and well adherent Ni deposits were obtained at -3.75 mA.cm^{-2} on the electrodeposited Cu substrate. This optimum current density was then pursued to try to deposit Ni on Al. The SEM image of the FIB milled region for this sample did not show a very clear contrast so an ion image was obtained as shown in Figure 22. It can be seen that on depositing Ni, Al got stripped away leaving behind porous deposits. These deposits are mainly Ni but the presence of some quantity of Al or Al-Ni alloy can be expected.

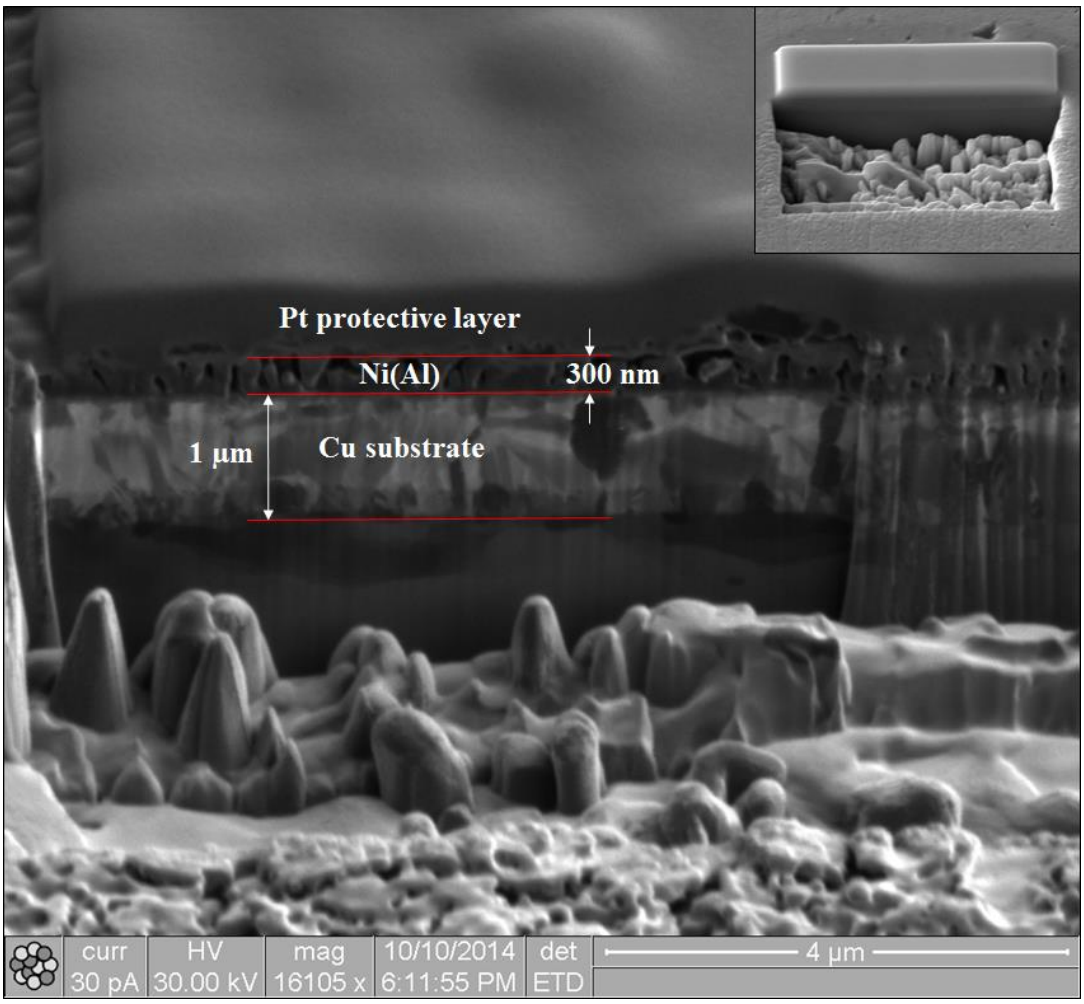

Figure 22. Ion image of a FIB cross-section of Al/Ni bilayer sample.

3.4 Conclusions

From the present study on the ED of Al-Ni and Al/Ni multilayers, the following conclusions can be drawn,

1. The concentration of Ni in electrodeposited Al-Ni alloys increases nonlinearly with the increase in molarity of $NiCl_2$. Al and Ni contents increase with increasing the time of positive and negative cycle of the pulse respectively. Decreasing the frequency by half resulted in almost double the amount of Ni in the deposited alloy. A smoother surface increased Ni concentration from 6 to 17.7 at.%.
2. The visual appearance of the deposits ranged from bright silver, dull silver, grey and black with a darker shade typically indicating higher Ni content. Al-Ni alloy typically showed nodular morphology with cauliflower structure. Flake structures, which were independent of surface roughness, were found to develop for 1:1 duty ratio. XRD on Al-Ni suggests the presence of supersaturated FCC crystalline solid solution of Al and Ni.
3. Dense and well adherent Pure Al and Ni were deposited at -0.3 and 0.5 V in AlCl3 -EMIM containing 0.026 M $NiCl_2$ showing very fine crystalline and cauliflower structures respectively.
4. Ni/Al bilayer was successfully deposited in 1.5:1 $AlCl_3$-EMIM containing 0.026 M $NiCl_2$. Deposition of Al on Ni was achieved, however, the deposition of Ni on Al is complicated due to the stripping of Al at the same potential at which Ni gets deposited.

CHAPTER 4: CONCLUSIONS AND FUTURE WORK

Electrodeposition of Al-Ni alloys and Ni/Al bilayer has been successfully demonstrated in this work. In chapter 2 it was described that dissolution of $NiCl_2$ in $AlCl_3$-EMIM room temperature melt was found to be favorable in basic electrolyte. A detailed study on the electrochemical properties of the electrolyte using cyclic voltammetry has been established. The use of an electrochemically active Cu WE effects the electrochemistry of the electrolyte by dissolving Cu in the scan range of 1 to 2 V and introducing additional oxidation and reduction peaks pertaining to the stripping and deposition of Cu. The current density of Ni and Al oxidation and reduction peaks varies directly and indirectly to the amount of $NiCl_2$ dissolved in the $AlCl_3$-EMIM electrolyte respectively.

In chapter 3 it was demonstrated that the concentration of Ni in Al-Ni alloy increased with the increase in amount of NiC_2 dissolved in the melt, increase in the time period of positive potential cycle, decrease in frequency and decrease in surface roughness of the WE. Al-Ni alloy typically showed nodular morphology with cauliflower structure. Flake structures, which were independent of surface roughness, were found to develop for 1:1 duty ratio. XRD on Al-Ni suggests the presence of supersaturated FCC crystalline solid solution of Al and Ni. Uniform Al/Ni bilayer was successfully deposited in 1.5:1 $AlCl_3$-EMIM containing 0.026 M $NiCl_2$. Deposition of Al on Ni was achieved while the deposition of Ni on Al has not been successfully possible yet in this electrolyte.

The collection of observations and findings in this thesis suggest a plethora of possibilities for further research. For instance studying the effect of other metals as WEs such as Ni, deposition of Ni on Al, Al/Ni nanopillars, electrodeposition of Al-Ni multilayer from other ionic liquids such as $AlCl_3$-BPC-$NiCl_2$ and application of these multilayers as self-propagating materials can pave the way for next generation engineering applications.

REFERENCES

[1] G. R. Stafford and C. L. Hussey, "Electrodeposition of transition metal-aluminum alloys from chloroaluminate molten salts," *Advances in Electrochemical Science and Engineering, Vol 7*, vol. 7, pp. 275-347, 2002 2002.

[2] A. Inoue, "Amorphous, nanoquasicrystalline and nanocrystalline alloys in Al-based systems," *Progress in Materials Science*, vol. 43, pp. 365-520, 12// 1998.

[3] M. Li, Z. Wang, and R. G. Reddy, "Electrodeposition of Nickel in 1-Butyl-3-Methylimidazolium Tetrafluoroborate Ionic Liquids," *Journal of The Electrochemical Society*, vol. 161, pp. D150-D153, January 1, 2014 2014.

[4] A. Inoue and H. Kimura, "Fabrications and mechanical properties of bulk amorphous, nanocrystalline, nanoquasicrystalline alloys in aluminum-based system," *Journal of Light Metals*, vol. 1, pp. 31-41, 2// 2001.

[5] F. Cai and C. Jiang, "Influences of Al particles on the microstructure and property of electrodeposited Ni-Al composite coatings," *Applied Surface Science*, vol. 292, pp. 620-625, Feb 15 2014.

[6] T. P. Moffat, "Electrodeposition of $Ni_{1-x}Al_x$ in a chloroaluminate melt," *Journal of the Electrochemical Society*, vol. 141, pp. 3059-3070, Nov 1994.

[7] M. R. Ali, A. Nishikata, and T. Tsuru, "Electrodeposition of Al-Ni intermetallic compounds from aluminum chloride-N-(n-butyl)pyridinium chloride room temperature molten salt," *Journal of Electroanalytical Chemistry*, vol. 513, pp. 111-118, Nov 2 2001.

[8] T. Egami and Y. Waseda, "Atomic size effect on the formability of metallic glasses," *Journal of Non-Crystalline Solids*, vol. 64, pp. 113-134, 1984 1984.

[9] T. Egami, "Universal criterion for metallic glass formation," *Materials Science and Engineering a-Structural Materials Properties Microstructure and Processing*, vol. 226, pp. 261-267, Jun 15 1997.

[10] T. Egami, "Atomistic mechanism of bulk metallic glass formation," *Journal of Non-Crystalline Solids*, vol. 317, pp. 30-33, Mar 2003.

[11] D. B. Miracle and O. N. Senkov, "Topological criterion for metallic glass formation," *Materials Science and Engineering a-Structural Materials Properties Microstructure and Processing*, vol. 347, pp. 50-58, Apr 25 2003.

[12] O. N. Senkov and D. B. Miracle, "Effect of the atomic size distribution on glass forming ability of amorphous metallic alloys," *Materials Research Bulletin*, vol. 36, pp. 2183-2198, Oct 1 2001.

[13] A. Inoue, H. Yamaguchi, T. Zhang, and T. Masumoto, "Al-La-Cu amorphous alloys with a wide supercooled liquid region," *Materials Transactions Jim,* vol. 31, pp. 104-109, Feb 1990.

[14] A. Inoue, T. Nakamura, N. Nishiyama, and T. Masumoto, "Mg-Cu-Y Bulk Amorphous Alloys with High Tensile Strength Produced by a High-Pressure Die Casting Method," *Materials Transactions Jim,* vol. 33, pp. 937-945, Oct 1992.

[15] S. J. Poon, G. J. Shiflet, F. Q. Guo, and V. Ponnambalam, "Glass formability of ferrous- and aluminum-based structural metallic alloys," *Journal of Non-Crystalline Solids,* vol. 317, pp. 1-9, 3// 2003.

[16] C. K. Kjartansdottir, L. P. Nielsen, and P. Moller, "Development of durable and efficient electrodes for large-scale alkaline water electrolysis," *International Journal of Hydrogen Energy,* vol. 38, pp. 8221-8231, Jul 9 2013.

[17] K. Higashi, "Positive exponent superplasticity in advanced aluminum alloys with nano or near-nano scale grained structures," *Materials Science and Engineering a-Structural Materials Properties Microstructure and Processing,* vol. 166, pp. 109-118, Jul 15 1993.

[18] M. Tacikowski, R. Sitek, K. Sikorski, and T. Wierzchon, "Structure of Al-Ni intermetallic composite layers produced on the Inconel 600 by the glow discharge enhanced-PACVD method," *Intermetallics,* vol. 17, pp. 1098-1104, Dec 2009.

[19] R. Sitek, K. Sikorski, J. Sobczak, and T. Wierzchon, "Structure and properties of the multilayers produced on Inconel 600 by the PACVD method with the participation of trimethylaluminum vapours," *Materials Science-Poland,* vol. 26, pp. 767-777, 2008 2008.

[20] R. Yamanoglu, "PRODUCTION AND CHARACTERIZATION OF Al-xNi IN SITU COMPOSITES USING HOT PRESSING," *Journal of Mining and Metallurgy Section B-Metallurgy,* vol. 50, pp. 45-52, 2014 2014.

[21] M. Sha, T. Wang, F. Bai, J. Li, and T. Li, "Simulation on solidification of an Al-Ni alloy under electromagnetic stirring," *China Foundry,* vol. 9, pp. 258-262, Aug 2012.

[22] J. A. Howell, S. E. Mohney, and C. L. Muhlstein, "Developing Ni-Al and Ru-Al intermetallic films for use in microelectromechanical systems," *Journal of Vacuum Science & Technology B,* vol. 29, Jul 2011.

[23] Y. Zhao and T. J. VanderNoot, "Electrodeposition of aluminium from nonaqueous organic electrolytic systems and room temperature molten salts," *Electrochimica Acta,* vol. 42, pp. 3-13, // 1997.

[24] T. Jiang, M. J. C. Brym, G. Dube, A. Lasia, and G. M. Brisard, "Electrodeposition of aluminium from ionic liquids: Part I - electrodeposition and surface morphology of aluminium from aluminium chloride (AlCl3)-l-ethyl-3-methylimidazolium chloride (EMIm Cl) ionic liquids," *Surface & Coatings Technology,* vol. 201, pp. 1-9, Sep 12 2006.

[25] T. Jiang, M. J. C. Brym, G. Dube, A. Lasia, and G. M. Brisard, "Electrodeposition of aluminium from ionic liquids: Part II - studies on the electrodeposition of aluminum from aluminum chloride (AICl(3)) - trimethylphenylammonium chloride (TMPAC) ionic liquids," *Surface & Coatings Technology,* vol. 201, pp. 10-18, Sep 12 2006.

[26] P. Coursol, G. Dufour, J. Cote, P. Chartrand, and P. Mackey, "Application of Thermodynamic Models for Better Understanding and Optimizing the Hall-Heroult Process," *Jom*, vol. 64, pp. 1326-1333, Nov 2012.

[27] S. Schaltin, M. Ganapathi, K. Binnemans, and J. Fransaer, "Modeling of Aluminium Deposition from Chloroaluminate Ionic Liquids," *Journal of the Electrochemical Society*, vol. 158, pp. D634-D639, 2011 2011.

[28] Q. Liao, W. R. Pitner, G. Stewart, C. L. Hussey, and G. R. Stafford, "Electrodeposition of aluminum from the aluminum chloride-1-methyl-3-ethylimidazolium chloride room temperature molten salt + benzene," *Journal of the Electrochemical Society*, vol. 144, pp. 936-943, Mar 1997.

[29] W. R. Pitner, C. L. Hussey, and G. R. Stafford, "Electrodeposition of nickel-aluminum alloys from the aluminum chloride-1-methyl-3-ethylimidazolium chloride room temperature molten salt," *Journal of the Electrochemical Society*, vol. 143, pp. 130-138, Jan 1996.

[30] T. Matsuda, S. Inoue, and T. Namazu, "Self-propagating explosive Al/Ni flakes fabricated by dual-source sputtering to mesh substrate," *Japanese Journal of Applied Physics*, vol. 53, Jun 2014.

[31] S. W. Kuk, H. J. Ryu, and J. Yu, "Effects of the Al/Ni ratio on the reactions in the compression-bonded Ni-sputtered Al foil multilayer," *Journal of Alloys and Compounds*, vol. 589, pp. 455-461, Mar 15 2014.

[32] I. Sraj, M. Vohra, L. Alawieh, T. P. Weihs, and O. M. Knio, "Self-Propagating Reactive Fronts in Compacts of Multilayered Particles," *Journal of Nanomaterials*, 2013 2013.

[33] A. K. Stover, N. M. Krywopusk, G. M. Fritz, S. C. Barron, J. D. Gibbins, and T. P. Weihs, "An analysis of the microstructure and properties of cold-rolled Ni:Al laminate foils," *Journal of Materials Science*, vol. 48, pp. 5917-5929, Sep 2013.

[34] T. S. Dyer, Z. A. Munir, and V. Ruth, "The combustion synthesis of multilayer NiAl systems," *Scripta Metallurgica et Materialia*, vol. 30, pp. 1281-1286, 5/15/ 1994.

[35] R. J. Gale, B. Gilbert, and R. A. Osteryoung, "Electrochemical and Spectral Investigations of Nickel(II) Ion Equilibria in Room-Temperature Chloroaluminate Solvents " *Inorganic Chemistry*, vol. 18, pp. 2723-2725, 1979 1979.

[36] C. L. Hussey, T. B. Scheffler, J. S. Wilkes, and A. A. Fannin, "Chloroaluminate Equilibria in the Aluminum Chloride-1-Methyl-3-ethylimidazolium Chloride Ionic Liquid," *Journal of the Electrochemical Society*, vol. 133, pp. 1389-1391, Jul 1986.

[37] C. C. Yang and C. P. Chang, "Aluminum Electrodeposition from Room Temperature Molten $AlCl_3$-BPC Salt Bath," *Journal of Marine Science and Technology*, vol. 1, pp. 31-37, 1993.

[38] J. Tang and K. Azumi, "Optimization of pulsed electrodeposition of aluminum from AlCl3-1-ethyl-3-methylimidazolium chloride ionic liquid," *Electrochimica Acta*, vol. 56, pp. 1130-1137, 1/1/ 2011.

[39] M.-J. Deng, I. W. Sun, P.-Y. Chen, J.-K. Chang, and W.-T. Tsai, "Electrode position behavior of nickel in the water- and air-stable 1-ethyl-3-methylimidazolium-dicyanamide room-temperature ionic liquid," *Electrochimica Acta*, vol. 53, pp. 5812-5818, Aug 1 2008.

[40] J. S. Wilkes, J. A. Levisky, R. A. Wilson, and C. L. Hussey, "Dialkylimidazolium chloroaluminate melts: a new class of room-temperature ionic liquids for electrochemistry, spectroscopy and synthesis," *Inorganic Chemistry,* vol. 21, pp. 1263-1264, 1982.

[41] Q. F. Li, H. A. Hjuler, R. W. Berg, and N. J. Bjerrum, "Influence of Substrates on the Electrochemical Deposition and Dissolution of Aluminum in $NaAlCl_4$ Melts," *Journal of the Electrochemical Society,* vol. 138, pp. 763-766, Mar 1991.

[42] D. F. Roeper, K. I. Pandya, G. T. Cheek, and W. E. O'Grady, "The Structure of Nickel Chloride in the Ionic Liquid 1-Ethyl-3-methyl Imidazolium Chloride/Aluminum Chloride: X-ray Absorption Spectroscopy," *Journal of the Electrochemical Society,* vol. 158, pp. F21-F28, 2011 2011.

[43] Y. G. Zhao and T. J. VanderNoot, "Electrodeposition of aluminium from room temperature AlCl3-TMPAC molten salts," *Electrochimica Acta,* vol. 42, pp. 1639-1643, 1997 1997.

[44] Q. X. Liu, S. Z. El Abedin, and F. Endres, "Electroplating of mild steel by aluminium in a first generation ionic liquid: A green alternative to commercial Al-plating in organic solvents," *Surface & Coatings Technology,* vol. 201, pp. 1352-1356, Oct 5 2006.

[45] S. Z. El Abedin, P. Giridhar, P. Schwab, and F. Endres, "Electrodeposition of nanocrystalline aluminium from a chloroaluminate ionic liquid," *Electrochemistry Communications,* vol. 12, pp. 1084-1086, Aug 2010.

[46] M. Ueda, H. Ebe, and T. Ohtsuka, "Electrodeposition of Al-Cr-Ni layer by pulse electrolysis in AlCl3-EMIC molten salt," *Electrochemistry,* vol. 73, pp. 739-741, Aug 2005.

[47] A. Bakkar and V. Neubert, "Electrodeposition and corrosion characterisation of micro- and nano-crystalline aluminium from AlCl3/1-ethyl-3-methylimidazolium chloride ionic liquid," *Electrochimica Acta,* vol. 103, pp. 211-218, Jul 30 2013.

[48] Q. X. Liu, S. Z. El Abedin, and F. Endres, "Electrodeposition of nanocrystalline aluminum: Breakdown of imidazolium cations modifies the crystal size," *Journal of the Electrochemical Society,* vol. 155, pp. D357-D362, 2008 2008.